

MAGNETIC AND SUPERCONDUCTING PROPERTIES OF



BY

Owolabi Taoreed Olakunle

A Thesis Presented to the
DEANSHIP OF GRADUATE STUDIES

KING FAHD UNIVERSITY OF PETROLEUM & MINERALS

DHAHRAN, SAUDI ARABIA

In Partial Fulfillment of the
Requirements for the Degree of

MASTER OF SCIENCE

In

PHYSICS

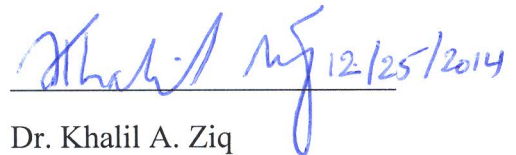
DECEMBER, 2014.

KING FAHD UNIVERSITY OF PETROLEUM & MINERALS

DHAHRAN- 31261, SAUDI ARABIA

DEANSHIP OF GRADUATE STUDIES

This thesis, written by **Owolabi Taoreed Olakunle** under the direction of his thesis advisor and approved by his thesis committee, has been presented and accepted by the Dean of Graduate Studies, in partial fulfillment of the requirements for the degree of **MASTER OF SCIENCE IN PHYSICS.**

 12/25/2014

Dr. Khalil A. Ziq
(Advisor)




Dr. Abdullah A. Al-Sunaid

Department Chairman



Dr. Salam A. Zummo
Dean of Graduate Studies



Dr. Shankar Kuwar
(Member)



Dr. Khalil Harrabi
(Member)

6/1/15

Date



©OWOLABI TAOREED OLAKUNLE

2014

Profound gratitude goes to Allah, for the invaluable gifts of life and wherewithal to complete the MS program.

ACKNOWLEDGMENTS

I am indebted to my advisor, Professor Dr. Khalil Ziq for his teaching, guidance, empathy and lessons of subconscious patience acquired during the course of undertaking this research in his group. I would like to express my gratitude to Dr. Khalil Harrabi, Dr. Shankar Kunwar and Dr. Ahmed F. Salem for being supportive during the course of this research. I also appreciate the patience exhibited by all the member of the committee during the course of undergoing this thesis work.

I would like to thank KFUPM institution for the scholarship granted to me to embark on my second degree program. I would also like to extend my gratefulness to the erudite faculty members of physics Department of the University for the paradoxical rigorous and appealing training in the discipline to complement my physics background.

Special thanks to my dear and near ones for being supportive since all these days, may Allah reward all with his paradise. Further, I wish to thank the host Kingdom of Saudi Arabia and the Nigeria community of an epoch in my autobiography of life-worthy semitic experience.

I would like to acknowledge NSTIP for funding this project under 11-ADV1631-04 project.

TABLE OF CONTENTS

ACKNOWLEDGMENTS	v
TABLE OF CONTENTS	v
LIST OF TABLES.....	xi
LIST OF FIGURES.....	x
ABSTRACT	xi
ABSTRACT ARABIC.....	xiv
1 CHAPTER 1 INTRODUCTION	1
1.1 Discovery of Superconductivity.....	1
1.2 Basic properties of superconductors	3
1.3 Classification of superconductors.....	4
1.4 Statement of the Problem addressed in this thesis work	4
1.5 Thesis Objectives	5
CHAPTER 2 LITERATURE REVIEW.....	6
2.1 History of Superconductivity.....	6
2.2 Iron Based Superconductor.....	7
2.2.1 Family of iron based superconductors.....	7
2.2.2 11-type iron base superconductor	8
CHAPTER 3 EXPERIMENTAL TECHNIQUE.....	10
3.1.1 Preparation of Q1 sample	10
3.1.2 Preparation of set Q2 samples.....	12
3.1.3 Preparation of set Q3 samples.....	15

3.2	Characterization of the fabricated samples.....	18
3.2.1	X-ray diffraction analysis	18
3.2.2	Magnetic measurement.....	18
3.2.3	Transport measurement using closed cycle refrigerator	20
CHAPTER 4 RESULT AND DISCUSSION.....		23
4.1	Results of X-ray diffraction analysis.....	23
4.1.1	Q1 Sample	24
4.1.2	Set Q2 sample	26
4.1.3	Set Q3 sample	34
4.2	Transport Measurement	39
4.3	Variation of magnetization with temperature for set Q2 samples	45
CHAPTER 5 MAGNETIC MEASUREMENTS		50
5.1	Temperature dependent of magnetic susceptibility for setQ3 samples	51
5.2	Magnetic properties.....	53
5.3	The critical current density.....	53
5.4	Pinning force.....	58
CHAPTER 6 CONCLUSION AND RECOMMENDATION.....		63
6.1	Conclusion	63
6.2	Recommendation for Future Work	64
References.....		65
Vitae.....		65

LIST OF TABLES

Table 3.1: The concentration of the constituents of set Q2 samples.....	.19
Table 3.2: The concentration of the constituents of set Q2 samples.....	.22
Table 4.1: Structural parameters of the non- superconducting phase.....	..31
Table 4.2: Structural parameters of tetragonal phase of set Q2 samples.....	37
Table 4.3: Structural parameters of the non- superconducting phase	38
Table 4.4: Structural parameters of set Q3 samples	43
Table 4.5: Structural parameters of the impurities phase of set Q3	50
Table 4.6: Magnetic transition temperature with conc. of As for set Q2.....	51

LIST OF FIGURES

Figure 3.1 Program rate of the furnace for set Q1 sample.....	12
Figure 3.2 Program rate of the furnace for set Q2 sample (First Annealing)	13
Figure 3.3 Program rate of the furnace for set Q2 sample (second Annealing)	14
Figure 3.4 Program rate of the furnace for set Q3 Samples	16
Figure 4.1 The Phase diagram of Fe-Se system^[9].....	24
Figure 4.2: X-ray diffraction pattern of set Q1- FeSe with plane indices.....	25
Figure 4.3: X-ray diffraction pattern of set Q2- FeSe with plane indices.....	27
Figure 4.4: X-ray diffraction pattern of FeSeAs 1% with plane indices	28
Figure 4.5: X-ray diffraction pattern of FeSeAs2% with plane indices	29
Figure 4.6: X-ray diffraction pattern of FeSeAs4% with plane indices	29
Figure 4.7: X-ray diffraction pattern of FeSeAs 6% with plane indices	30
Figure 4.8: X-ray diffraction pattern of FeSeAs 8% with plane indices	30
Figure 4.9: X-ray diffraction pattern of FeSeAs10% with plane indices	31
Figure 4.10a: Variation of lattice parameter with con. setQ2(hexagonal)	35
Figure 4.10a: Variation of lattice parameter with con. setQ2(hexagonal).....	32
Figure 4.10b: Variation of lattice parameter with con. setQ2(Tetragonal).....	32
Figure 4.11: X-ray diffraction pattern of FeSe with plane indices	36
Figure 4.12: X-ray diffraction pattern of FeSeAs 0.5% with plane indices.....	36
Figure 4.13: X-ray diffraction pattern of FeSeAs 1% with plane indices	37
Figure 4.14: X-ray diffraction pattern of FeSeAs 3%with plane indices	37
Figure 4.15: Variation of lattice parameters with arsenic Con. for set Q3_FeSe.....	41
Figure 4.16: Structural transition observed in FeSe superconductor^[10]	42
Figure 4.17: Transport measurement for set Q2_FeSe	42
Figure 4.18: Structural transition on Set Q2	43
Figure 4.19: Transport measurement for set Q2_FeSeAs 6%	40
Figure 4.20: Transport measurement for set Q2_FeSeAs 8%	44
Figure 4.21: Transport measurement for set Q2_FeSeAs 10%	47
Figure 4.22: Derivation of resistivity with temperature for set Q2 samples.....	47
Figure 4.23: Magnetization dependent temperature for set Q2 (0% and1%).....	49
Figure 4.24: Magnetization dependent temperature for set Q2 samples.....	49
Figure 4.25: Variation of magnetic moment with temperature	48
Figure 4.26: Phase diagram of FeSeAs-system	49
Figure 5.1: Magnetization against applied field for Set Q2_FeSeAs0%.....	52
Figure 5.2: Magnetization against applied field for Set Q2_FeSeAs @ 4K.....	52
Figure 5.3: Magnetization against applied field for Set Q2_FeSeAs at 8K	53

Figure 5.4: Critical current density at different temperature for set Q2_FeSeAs ...55
Figure 5.5: Critical current density at different temperature for Q2_FeSeAs1% ...56
Figure 5.6: Current density at different temperature for set Q2_FeSeAs for 6%As57
Figure 5.7: The variation of critical current density for Set Q2_FeSeAs at 4K58
Figure 5.8: Variation of the pinning force with the applied field for set Q2_FeSe60
Figure 5.9: The pinning force with the applied field for set Q2_FeSeAs 1% of As60
Figure 5.10: The pinning force with the applied field for set Q2_FeSeAs 6% of As ..61
Figure 5.11: The variation of the pinning force for Set Q2_FeSeAs system at 4K....61

ABSTRACT

Full Name : Owolabi Taoreed Olakunle

Thesis Title : Magnetic and superconducting Properties of Fe(SeAs)

Major Field : Physics Department

Date of Degree : December, 2014

The effects of arsenic substitution on the structural, transport, magnetic and superconducting properties of FeSe were investigated. X-ray diffraction, resistivity and magnetic measurements performed on $\text{FeSe}_{1-x}\text{As}_x$ have been used to obtain the structural, magnetic and superconducting transition temperatures. We found that low concentrations of arsenic (~1%) substitution promote the hexagonal phase and the appearance of weak magnetic behavior with very little effect on the superconducting transition. Moreover, above 6% of arsenic substitutions, FeSe experiences total loss of superconductivity and ferromagnetic like behavior becomes stronger. Magnetic measurements revealed reductions in both critical current density and pinning forces at low arsenic content. However, the critical current density and pinning force slightly improve as the concentration of arsenic increases. Consequent: structural, magnetic and superconducting transition temperatures have been used to generate the phase diagram of $\text{FeSe}_{1-x}\text{As}_x$ as upon varying the arsenic concentration.

ملخص الرسالة

الاسم الكامل: توريد أوكونلي أولابي

عنوان الرسالة: الخصائص المغناطيسية وفائقة الموصلية ل $\text{FeSe}_{1-x}\text{As}_x$

التخصص: فيزياء

تاريخ الدرجة العلمية: December, 2014

تم في هذا البحث استقصاء تأثير إضافة الزرنيخ على كل من التركيب البلوري والخصائص المغناطيسية والمفرطة الموصلية للواد $(\text{FeSe}_{1-x}\text{As}_x)$ حيث $(x < 0.1)$. استخدمنا تقنية تشتت الأشعة السينية والقياسات المغناطيسية وقياس المقاومة الكهربائية لتحديد التركيب البلوري ودرجات حرارة الانتقال التطوري. وجدنا اننا نحتاج الى نسبة ضئيلة ($\approx 1\%$) من الزرنيخ لتكوين طور التركيب البلوري السداسي والتي عندها يظهر سلوكا مغناطيسيا ضعيفا، مصاحبا ذلك أثرا ضئيلا على فرط الموصلية. وعندما تصل نسبة الزرنيخ الى 6% فإن الخصائص الفرو-مغناطيسية تزداد وتختفي عندها خصائص فرط الموصلية.

أظهرت القياسات المغناطيسية على العينة عند تركيز منخفض (1%) من الزرنيخ حدوث نقصان في كثافة التيار الحرج وقوة التثبيت. لكن عند زيادة تركيز الزرنيخ قليلا وجد تحسن وزيادة في قيمة كل منهما. بناء على نتائج قياس درجات الحرارة الانتقالية -مغناطيسية، تركيبية وفرط الموصلية- تمكننا من وضع رسم الشكل البياتي للطور لمادة $(\text{FeSe}_{1-x}\text{As}_x)$.

CHAPTER 1

INTRODUCTION

1.1 Discovery of Superconductivity

The trend of accidental discovery of superconductivity that started in 1911 in Leiden University by a Dutch Physicist extends to the recently (2008) discovered iron based superconductors. Heike Kamerlingh Onnes, the Dutch Physicist, was investigating the behavior of the residual resistivity of high purity mercury when he accidentally discovered superconductivity. More recently; Hideo Honoso of Toyko Institute of technology desired to fabricate transparent semiconductor, he stumbled on a new type of superconducting material; the Iron based [1]. The theoretical explanation of superconductivity was introduced in 1957 by John Bardeen, Leon Cooper and Robert Schrieffer. Their theory is commonly known as the BCS theory [2] is based on the idea of electron-phonon coupling to bind two electrons in pairs known as the cooper pairs. These cooper pairs are responsible for creating the superconducting state. The theory explained several properties of the superconducting material such as the occurrence of the energy gap in the density of states and the isotopes effects.

Superconducting materials that follows the BCS theory are often known as conventional superconductors; their transition temperatures are around 20 K.. Surprisingly, the new class of ceramic copper oxide superconductors were discovered in 1986 by Bendnorz and Muler. Since all of these materials have common copper oxide layers, which are believed to be

responsible for superconductivity, they are called cuprate superconductors. The parent compounds of the cuprate superconductors are special type of insulators known as Mott insulators. However, these materials can turn superconducting at certain transition temperature (T_c) while either hole or electrons are doped. The transition temperature of these materials is quite higher than the maximum T_c predicted by BCS theory. Therefore they are unconventional and are also known as high T_c cuprate superconductors. While the mechanism of superconductivity in high T_c cuprates is still unknown and under debate, a new set of unconventional superconducting materials were discovered in 2008 by [1]. The common element of these new set of superconductors is iron so they are called iron based superconductors. One of such iron based superconductors, namely FeSe, is the main focus of this thesis.

Recent discovery of the Fe-based superconductors revived new interest and research in superconductivity [4]. Iron being ferromagnetic hinders the formation of cooper pairs in conventional superconductors. Locally polarized spins present in ferromagnetic materials (such as iron) whose magnetic field is liable to distorts the formation of cooper pairs, appeared to be a setback to Dirk Johrendt and his group when they suspected superconductivity in ferromagnetic materials ($SrRh_2P_2$ and $SrCo_2P_2$) in the mid-1990 [5]. . Several Fe-based superconducting families have been discovered since its initial discovery.[6]. The simplest of these family is the FeSe family commonly known as the Fe-11 [7-13]. The simplicity in the crystal structure of FeSe which allows diverse doping mechanisms makes it attractive material to investigate diverse superconducting, magnetic and transport properties [9]. One of the main concerns in preparing FeSe material is to stabilize the tetragonal structure that gives the superconducting phase. It has been found that

excess Fe atoms in Fe_{1+x}Se occupy interstitial positions in the structure and help stabilizing the tetragonal phase. Similar effect has been found by creating vacancies at the Se-sites when using Se deficiency in FeSe_{1-x} . In such case Fe-atoms may occupy these vacancies and help stabilizing the tetragonal structure [10-11].

There are two basic structures in FeSe-system; hexagonal (α and δ) and tetragonal (β). Superconductivity occurs in the tetragonal β -phase with transition temperature of 8-12 K with PbO structure. It also exists as hexagonal which can be either superconducting (α) or non-superconducting δ -phase [9]. Non-superconducting hexagonal phase exists at a temperature around 1075°C as depicted in the binary phase diagram while the hexagonal superconducting phase forms below 450°C .

This thesis work aims at preparing and characterizing specific phase of FeSe using partial substitutions of arsenic. Transport measurement, magnetic measurements and X-ray diffraction technique are used in this investigation, ultimately obtaining the phase diagram of $\text{FeSe}_{1-x}\text{As}_x$.

1.2 Basic properties of superconductors:

There are two basic properties that uniquely characterize superconducting materials; namely: loss of resistance below certain critical temperature known as the superconducting transition temperature, and; perfect diamagnetic behavior below the certain critical applied magnetic field. This is commonly known as the Meissner effect. This effect clearly distinguishes superconductors from perfect conductors.

Most of the practical applications of superconducting materials are based on proper utilization of these properties. The temperature below which a material can super-conducts or above which

a material loses its superconductivity is known as the **critical temperature**. The higher the critical temperature the more suitable is the material for practical applications. Below this temperature, there is a maximum current density that a superconductor can carry in order to maintain its superconductivity; current density higher than will destroy the superconducting state. This means that higher current are desirable for many application.

1.3 Classification of superconductors

Superconductors are commonly classified using several approaches. By the virtue of their responses to magnetic field, those with single critical field above which the superconductivity is lost are referred to as type I superconductors. Type II superconductors are characterized with two critical fields [12], between which partial penetration of magnetic field occurs in the superconducting state creating the “mixed state”. Another mode of classification is by using the term “conventional” and “non –conventional”, depending on whether it can be explained by BCS theory or not. In conventional superconductors, the electron-electron interaction is mediated by phonon in a accordance with the BCS theory. While there is no clear-cut specific transition temperature to distinguish high temperature superconductors (HTcS) from low temperature superconductors; initially; materials with superconducting transition ~ 30 K are classified as high temperature superconductor.

1.4 Statement of the Problem addressed by this thesis work

In this thesis, substitution effects of arsenic at the Se-site in FeSe superconducting material is being investigated. We used several preparation techniques in an effort to stabilize certain structure (Hexagonal and tetragonal).

1.5 Thesis Objectives

The specific objectives of this research thesis include:

1. To obtain the phase diagram for As doped FeSe superconductor.
2. To study the effect of As on the critical current density and pinning forces in $\text{FeSe}_{1-x}\text{As}_x$
3. To obtain the optimal conditions that stabilizes tetragonal and hexagonal phases.

CHAPTER 2

LITERATURE REVIEW

2.1 History of Superconductivity

The phenomenon of superconductivity came into being when Heike Kamerlingh Onnes investigated the resistivity of pure mercury with temperature in 1911. He found that the resistivity of mercury drops to zero at 4 K. This is in clear contradistinction to the widely accepted Drude behavior of the resistance. In 1933 Walther Meissner and Robert Ochsenfeld investigated the magnetic properties of this class of material. They showed that below this critical temperature, superconductor expels magnetic field from its interior and allows no field penetration below certain critical magnetic field H_c . This effect, called Meissner effect is not present in perfect conductors; it is a unique property of superconducting material.

The first explanation of superconductivity came into existence in 1957 when three American Physicists, John Bardeen, Leon Cooper and Robert Schrieffer came up with a theory of electron-electron coupling through phonon mediated interaction (cooper pairs) as a mean to explain superconductivity [2]. Their theory is commonly known as the BCS theory.

Perovskites, a class of metal oxide ceramics, was found to be superconducting by Georg Bednorz and Alex Muller in 1986 in Switzerland [3]. Superconductivity was found in perovskite material in February 1987 at 90 K and this marked a new era in research in superconductors and their applications. These superconductors are known as high temperature

Superconductor because of their ability to transit to superconducting phase at temperatures higher than the highest transition temperature in conventional superconductor.

In 2008 a new class of superconducting materials has been discovered, the Fe-based superconductor. This discovery revived the hope of reaching room temperature superconductivity.

2.2 Iron Based Superconductor

Iron, the fourth common element in the earth crust has formed the major constituent of compounds in which superconductivity was discovered [13]. The Iron Age replaces that of copper era due to rising in critical magnetic field as well as high isotropic critical current attached to iron based superconductors. One of the unique properties of iron based superconductor is the coexistence of superconductivity and ferromagnetism. Soon after the discovery, the transition temperature was raised to 26 K in $LaFeAsO_{1-x}F_x$ by merely replacing phosphorus with arsenic and part of oxygen with fluorine in the 1111-type of iron based superconductor with a chemical formula $RFeAsO$ [1]. Various Fe-based superconducting families presented in the following section.

2.2.1 Family of iron based superconductors

There are several families of the iron-based superconductors. They are grouped according to the atomic ratio of the constituent elements composing the superconducting material. Their main members are:

- (a) 122-type ($BaFe_2As_2$): The first member of this family was discovered and fabricated in Ludwig-Maximilians university in Germany by Dirk Johnrendt and his group [5].

Although, Dirk Johnrendt had suspected superconductivity in a ferromagnetic compound in mid-1990 but he was set aback because of his view that formation of cooper pairs could be hindered by the field of ferromagnetic materials. In this family, alkaline earth metals interlayered the corrugated layers of iron and arsenic. Several doping of iron with other elements such as cobalt improves transition temperature of these materials [5].

(b) 1111-type ($RFeAsO_{1-x}F_x$): In this family, the parent compound (i.e. corrugated layer of FeAs) is interlayered by rare earth element (R) and oxygen. They have the highest transition temperature (~55 K) among the Fe-based superconductors. Their critical temperature rises upon doping with fluorine [1].

(c) 111-type (LiFeAs): This family consists of alkali metals (such as lithium) as the interlayer element [14]. The first member of the family was discovered simultaneously by three different groups in three continents [5].

(d) 11-type (FeSe): This is the simplest family of iron based superconductor [21-23] came into existence due to safety precaution embarked on by the academia sinca's institute of physics in Taipei. Maw-kuen removed trivalent arsenic and monovalent lithium from the lattice structure of 111-type and balanced it with divalent less toxic selenium [5]. In this thesis we will be investigating the structure, magnetic and transport properties of this family.

2.2.2 11-type iron base superconductor

FeSe is heavily studied superconducting material due to its simple structure that allows several doping elements to be incorporated in the structure [27-32]. The binary phase diagram of this alloy reveals a rather complicated and various possible phases at different temperatures. The

prepared FeSe material often found to contain 3-mixed structures: the α -phase (tetragonal), β - and δ -phases (both are hexagonal structure). Out of these phases, α and β are superconducting phase [29- 32].

Iron forms magnetic clusters around the vacancies created by selenium which gives rise to the superconductivity observed in this material [21]. Moreover, excess Fe-atoms stabilizes the tetragonal phase in this compound and enhances the appearance of superconductivity in FeSe [22]. The emergence of superconductivity occurs in a narrow range of the atomic ratio close to the ideal stoichiometry (that is, 1:1). Upon cooling; FeSe undergoes structure transition from tetragonal to orthorhombic near 70 K [23].

Optimizing preparation techniques that leads to enhancing or favoring the growth of any of these phases is one of the goals of this thesis. Several literatures reveal that the superconducting transition temperature of FeSe falls within 8- 10 K for poly or single crystalline, and could reach 12 K in thin film material [25,32]. The application of high pressure was found to enhance the transition temperature reaching about 27 K and 37 K under 1.5 GPa and 8.9 GPa respectively [31-32] Furthermore, the method of fabricating these materials play a significant role in affecting the transition temperature as well as other superconducting and magnetic properties. Significantly transition temperature of 65 K was observed in FeSe system grown on selenium-etched SrTiO₃ substrate using molecular beam epitaxy [27-28].

In this research work, we investigated the effect of arsenic substitutions on the magnetic and superconducting properties of FeSe-system and finally established its phase diagram.

CHAPTER 3

EXPERIMENTAL TECHNIQUE

3.1 Preparation of $\text{FeSe}_{1-x}\text{As}_x$ samples

Solid state reaction has been used to prepare stoichiometric ratios of all samples ($\text{FeSe}_{1-x}\text{As}_x$) used in this work. High purity (99.99%) elements were used. Three different sets of samples were prepared using different annealing and quenching procedures. These are:

1. $\text{FeSe}_{1-x}\text{As}_x$ samples annealed at 1050°C and further quenched from 700°C to the room temperature (known as Q1)
2. $\text{FeSe}_{1-x}\text{As}_x$ samples prepared by annealing at 700°C and 400°C (known as Q2)
3. $\text{FeSe}_{1-x}\text{As}_x$ samples annealed at 800°C and quenched from 350°C to the room temperature (known as Q3).

1. Preparation of set Q1 sample

The purpose of preparing this sample is to investigate the quenching and annealing temperature that favor the emergence of any of the three structural phases (α , β and δ phase) as given earlier for FeSe alloy. The concentration of arsenic was set to zero in this case.

Prior to the solid state reaction between Fe and Se, iron powder was further purified by removing any oxide surface layer. This was achieved by annealing the powder for about 20 minutes at 400°C in hydrogen-argon atmosphere (ratio 1:9 respectively). This has been found sufficient to remove the iron oxide at the surface of the Fe-grains, hence producing iron with

high purity content (~99.99%). The argon (an inert) gas was used to prevent hydrogen combustion during annealing. The purified iron is being used in the preparation of all samples used in this thesis.

Appropriate amounts (stoichiometric ratios) of iron powder (Fe) and Selenium (Se) were mixed to produce one gram of FeSe sample. The combined elements were mixed and grinded to fine powder using small mortar and pestle, pressed into pellets and then sealed in a quartz tubes under partial atmospheric pressure (20-25%) of argon. The sample (FeSe) was annealed at 1050°C for 24hr in a programmable furnace in accordance to the chart shown in figure 3.1a. The heating rate was kept low (60°C/hr) to avoid thermal shock and give more time for the reaction to take place at low temperatures (Se melts at ~220°C). The samples were cooled to 700°C slowly at a rate of 20°C/hr to stabilize the δ -phase formed at high temperature. The sample was annealed at 700°C for another 24hr was then quenched (fast cooling) to the room temperature using by dropping the quartz tube water bath. Quenching preserves the structural phases that have been stabilized at high temperature (700°C) room temperature.

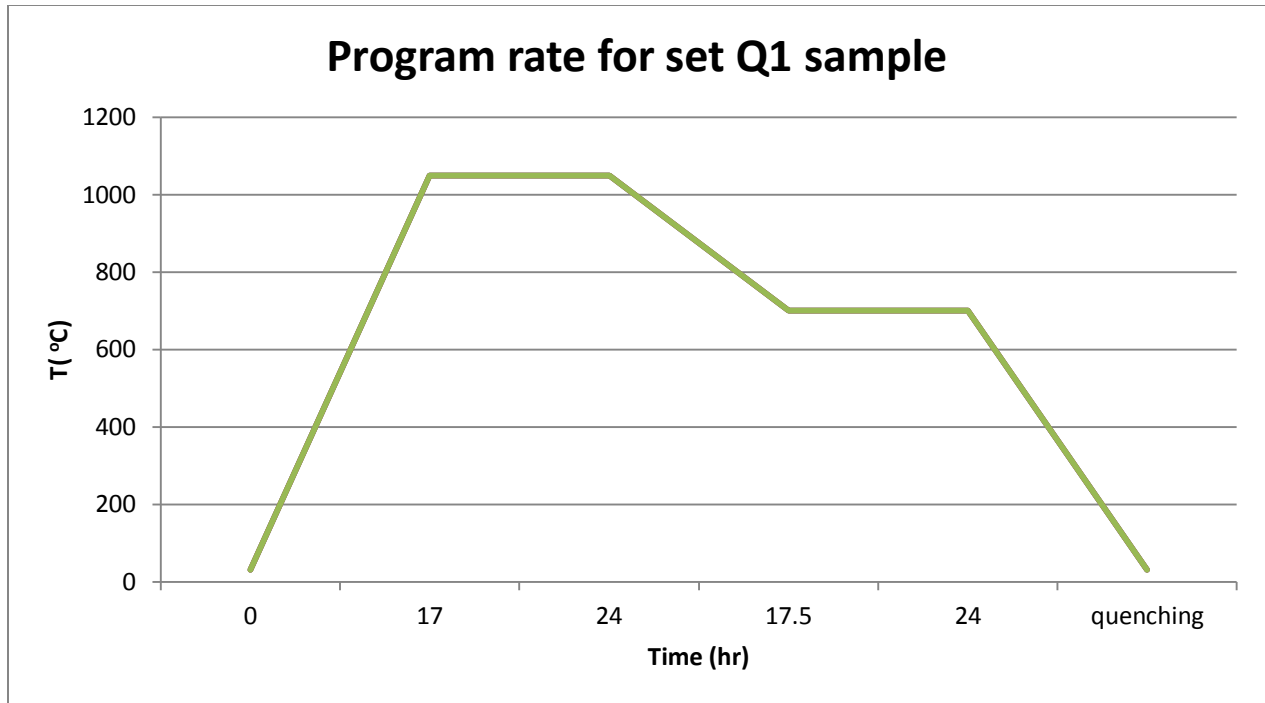


Figure 3.1 Program rate of the furnace for set Q1 sample

3.1.2 Preparation of set Q2 samples

The x-ray diffraction characterization carried out on Q1 sample shows the absence of superconducting phase (the details are presented in the next chapter) which calls for further improvement in the fabrication processes. In order to explore other annealing procedures through which the superconducting phase of FeSe material could be enhanced and favored, another set of samples ($\text{FeSe}_{1-x}\text{As}_x$) were prepared using two steps processes. The samples were slowly cooled to room temperature. The purified iron powder was mixed with selenium and arsenic powder to form one gram of six samples with different concentration of arsenic as presented in table 3.1. Each of the six samples was grinded and mixed together using small mortar and pestle, pressed into pellets and then sealed in quartz tubes under partial pressure of argon (20-25%).

All samples were annealed in programmable furnace in accordance to the chart presented in figure 3.2. The furnace was programmed to raise the temperature of the sample from the room temperature up to 200°C at the rate of 60°C/hr and stays at 200°C for 24hr before begins to rise again at rate of 60°C/hr until it attains a temperature of 500°C, then annealed for 24hr. The temperature was raised to 700°C (rate of 60°C/hr) and annealed for another 24hr. The samples were furnace cooled to the room temperature.

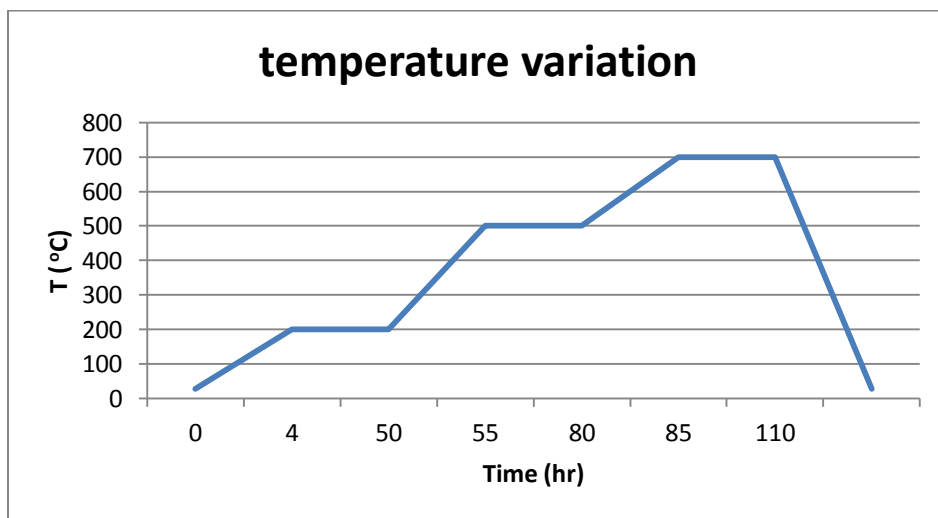


Figure 3. 2 Program rate of the furnace for set Q2 sample (First Annealing)

After the first annealing process, each sample was grinded and mixed pressed into pellet, further sealed under partial pressure of argon and annealed at low temperature for the second time. Heating rate has been kept at 60°C/hr as before.

Initially the samples were annealed at 200°C 5hr, then at 400°C in 10hr and then slowly cooled down to room temperature without quenching. The programming pattern of the furnace is presented in figure 3.3.

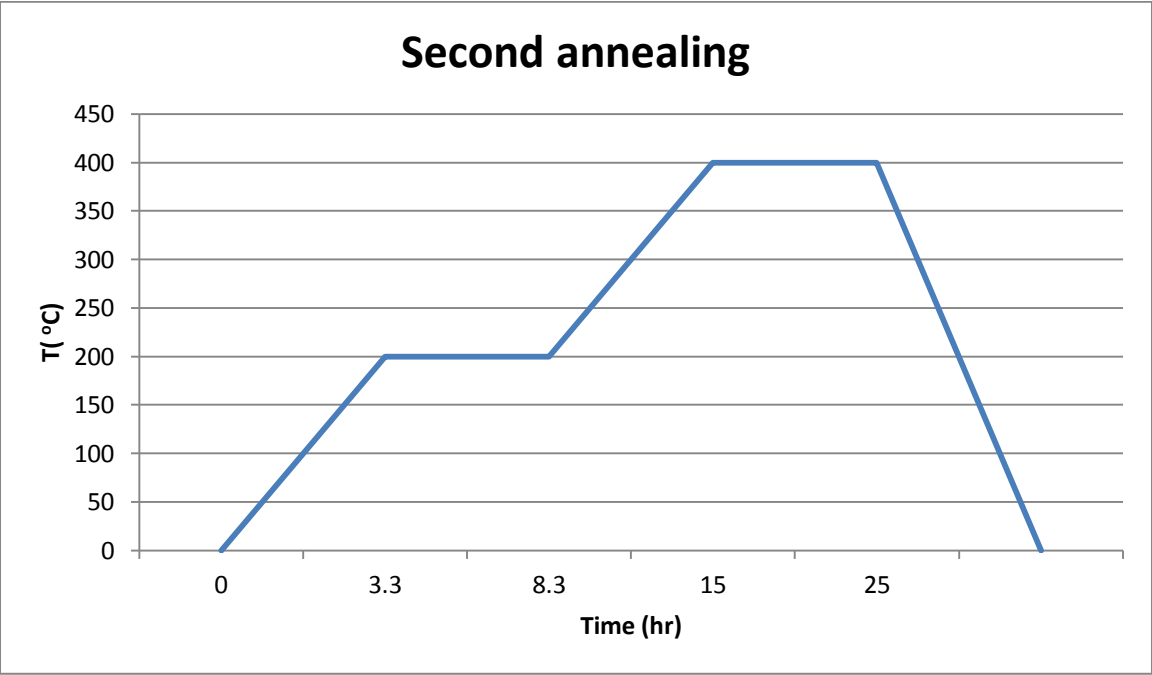


Figure 3. 3: Program rate of the furnace for set Q2 sample (second Annealing)

Table 3.1: The concentration of the constituents of set Q2 samples

			In gram	In gram	In gram	In gram	In gram
Sample	x	1-x	mwt	Fe	As	Se	FeSe _{1-x} As _x
Sample 1	0.01	0.99	134.7646	0.4144	0.0056	0.5798	0.9997
Sample 2	0.02	0.98	134.7242	0.4145	0.0111	0.5741	0.9997
Sample 3	0.04	0.96	134.6435	0.4148	0.0223	0.5627	0.9997
Sample 4	0.06	0.94	134.5627	0.4150	0.0334	0.5513	0.9997
Sample 5	0.08	0.92	134.4819	0.4153	0.0446	0.5399	0.9997
Sample 6	0.1	0.9	134.4012	0.4155	0.0557	0.5285	0.9997

3.1.3 Preparation of set Q3 samples

After performing several transport, structural and magnetic measurements, it was noticed that a more detailed study is needed for the low arsenic concentration ($x < 0.04$). We followed similar heat treatment as in set Q2 samples, with slightly different annealing temperatures. To improve on the accuracy of the concentration of low arsenic content, samples were prepared from FeAs and FeSe rather than from the elements as starting materials. This reduces the relative error in

weighing small quantities. Appropriate ratio to obtain the stoichiometric samples has been used as given in table 3.2.

All samples were annealed in accordance to the chart presented in figure 3.4. The heating rate was kept at $120^{\circ}\text{C}/\text{hr}$. First, the samples were annealed at 200°C for 2hrs, then at 300°C for 10hr and then annealed at 600°C for another 10 hrs. The samples were annealed at 800°C for 20hr before they were cooled ($120^{\circ}\text{C}/\text{hr}$) to 350°C and annealed for 100hr. At this temperature, the samples were quenched to the room temperature using water bath.

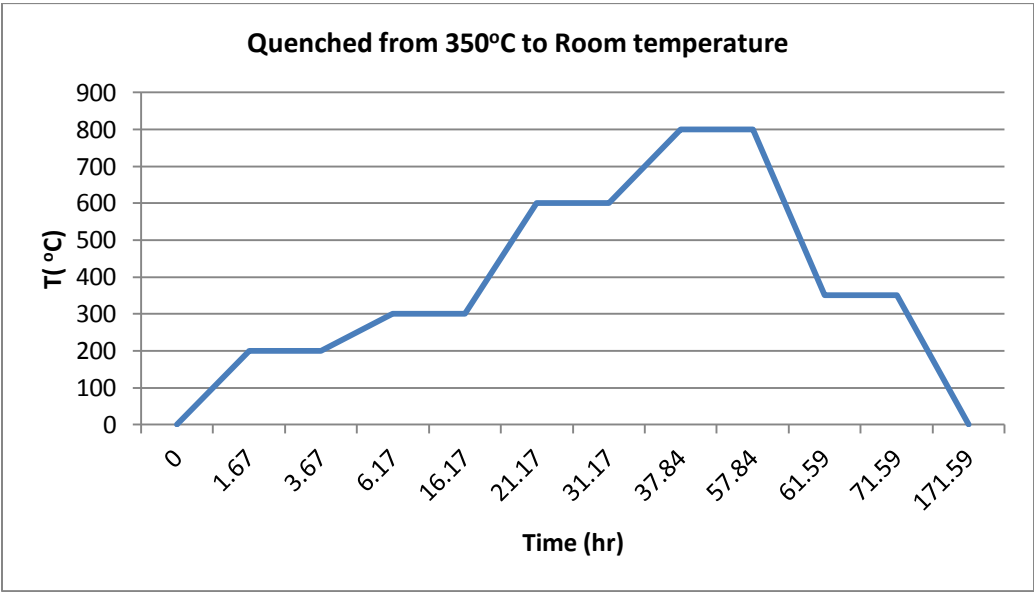


Figure 3. 4 : Program rate of the furnace for set Q3 Samples

Table 3.2: The concentration of the constituents of set Q2 samples

Element	Molecular Weight(g)	5g of FeSe	
Fe	55.8450	2.0713	
Se	78.9600	2.9287	
As	74.9216		Total(FeSe)
FeSe	134.8050		5g
FeAs	130.7666		
	1g of FeAs		
Fe	0.4271		
As	0.5729		
		Total(FeAs)	
		1g	
FeSeAs(1g)	FeSe(g)	FeAs(g)	FeSeAs(g)
0% As	1.0000	0.0000	1
0.5% As	0.9951	0.0049	1
1% As	0.9903	0.0095	1
3% As	0.9709	0.0291	1

3.2 Characterization of the fabricated samples

Each set of the prepared samples were subjected to three main characterization technique, which are described as follow.

- a. X-ray diffraction analysis.
- b. Magnetic measurement using 9-tesla vibrating sample magnetometer (VSM).
- c. Transport measurement using closed cycle refrigerator.

3.2.1 X-ray diffraction analysis

Crystal's structures were determined using powdered x-ray diffraction technique using Rigaku MiniFlex. The powdered samples were packed in a silicate glass. Silicate glass holder does not have any x-ray diffracted peaks that overlaps with peaks coming from the studied samples, hence completely eliminates the ambiguity that might be present is identifying the true crystal structure of the sample.

All sets of samples prepared in this research work were characterized using x-ray diffraction technique and the graphs of the intensity against 2θ were plotted for each sample. The structural parameters of the samples were estimated using the Brag's law in equation (1).

$$2d \sin \theta = n\lambda \quad (1)$$

3.2.2 Magnetic measurement

All magnetic measurements were performed on vibrating sample magnetometer (VSM) upon varying either the temperature or applied magnetic field. PAR (4500) and Quantum Design

VSM have been used in this thesis and presented in figure 3.5. The working principle of the VSM is based on vibrating the samples in a given magnetic field. The applied magnetic field aligns the magnetic domains or magnetic spins of the magnetic sample with the field. The sample is considered as a magnetic dipole that moves with sinusoidal movement; the magnetic dipole causes a time dependent change in the magnetic flux through a set of pick-up coils. According to Faraday’s principle, varying magnetic flux induces emf through the pick-up coils. Moreover; the induced voltage is proportional to the magnetization of the sample. .

The greater the magnetization of the magnetic dipole (to the constant magnetic field), the greater the induced current/voltage in the coils. The induced current can then be amplified and calibrated using magnetic known materials standard sample. The graph of magnetization at various temperatures in a known magnetic field, or its variations with the applied field at given temperature can easily be generated through computer controlled procedure and software available with both system used in this research.

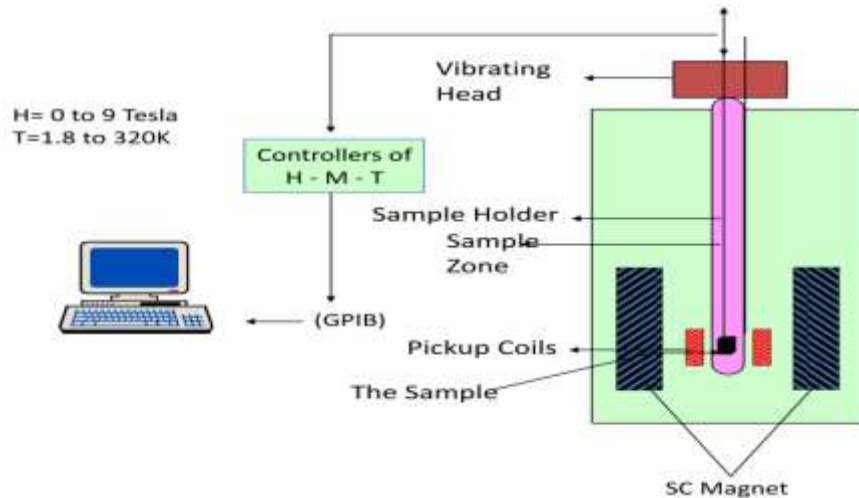


Figure 3.5: Experimental set up for the magnetic measurement

In the case of our prepared samples, magnetic measurements were carried out in a 9-tesla VSM in the temperature range (4.2-20 K). The magnetometer was calibrated using a Ni-standard, and the temperature stability was better than 0.1 K.

Magnetic measurements were also carried out on set Q3 samples in a 14-tesla VSM (physical properties measurement system, Quantum Design) in the temperature range (4-20 K). The magnetometer was calibrated using a Palladium-standard, and the temperature stability was better than 0.1 K. The reference sample was taken through field cooling and zero field cooling modes at 200e magnetic field with temperature range from 4 K to 20 K and 20 K to 4 K respectively.

3.2.3 Transport measurement using closed cycle refrigerator

Resistivity measurement was carried out in a closed cycle refrigerator (8200 compressor, CTI Cryogenics) with the aid of four probe technique. The closed cycle refrigerator is connected with nano-voltmeter (Hewlett 34420A), high current source measure unit (Keithley 238), temperature controller (Lakeshore 330), cryostat confined inside external magnet, computer system, and pumps (mechanical and diffusion pump) as shown in figures 3.6 and 3.7. The connected instruments enhanced the resistance of our prepared superconducting samples to be measured from room temperature to 14 K.

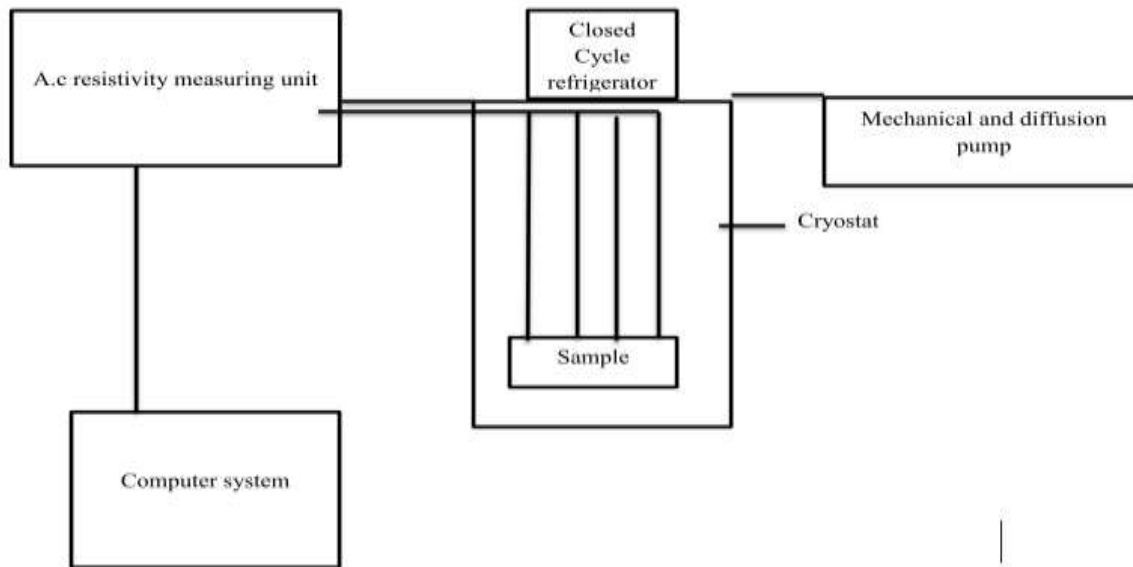


Figure 3.6: Experimental set up for the transport measurement (d.c set up)

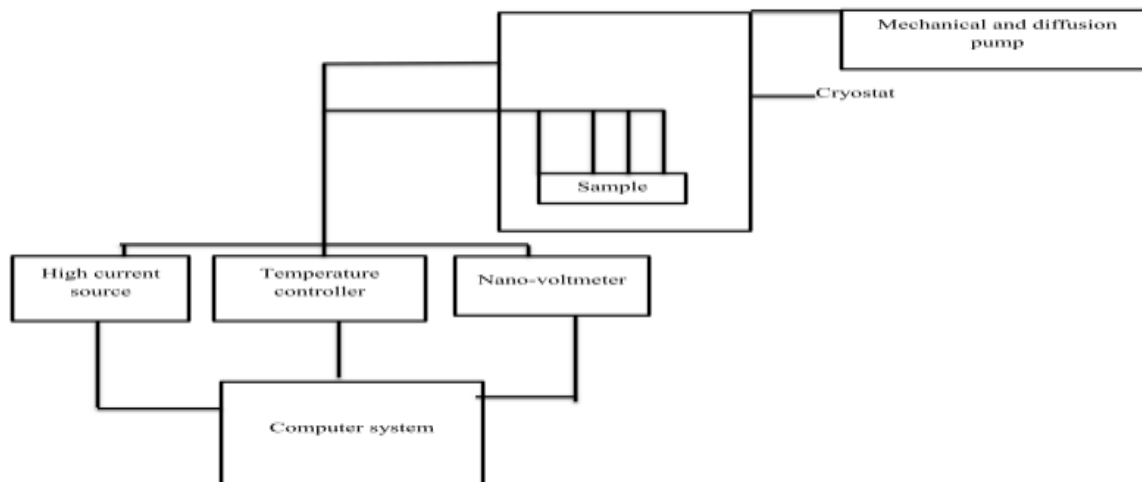


Figure 3.7: Experimental set up for the transport measurement (a.c set up)

In our system, there are two connecting pumps, rough pump and diffusion pump. The rough pump takes the system to about 10^{-3} mbar before the operation of diffusion pump which helps in evacuating the system up to 10^{-6} mbar.

The refrigerator also connected directly to high current source measure unit (Keithley 238) and nano-voltmeter that measures current passing through the sample as well as the potential difference between two terminals of the sample respectively. With this arrangement, the resistance of the sample could be measured at different temperature with the using four probe technique..

The transport measurements conducted on the superconducting samples prepared in this thesis work involved utilization of four-probe technique which eliminates the contact resistance. Charges accumulation and capacitance effects are eliminated by using constant-AC-current source. It has been found that using about 10-50 mA AC current is sufficient to destroy any thin layer oxide that may form between the terminals and the surface of the sample. In the ac-resistivity setup (LR-750) the frequency of a.c current was maintained at 17 Hz throughout the measurement. The four terminals that connect the samples were connected to the cold finger of the cryostat with the two terminals for measuring current and the other two for measuring potential different between two points. The measured current and voltage are amalgamated to obtain the resistance of the sample using LABVIEW software.

CHAPTER 4

RESULT AND DISCUSSION

4.1 X-ray diffraction analysis

X-ray diffraction patterns and analysis has been carried out all Q1, Q2 and Q3 samples.

Before proceeding to the analysis of x-ray diffraction results, it is crucial to discuss the binary phase diagram which has been used as a guide to the annealing and quenching procedures adopted for preparations of FeSe alloy. The binary phase diagram is a display of various stable phase for a given binary system at a given composition and temperature. The preparation of all sets of our superconducting samples involves three high purity elements (Iron Fe, Selenium Se and Arsenic As). Various concentrations of arsenic element are introduced into crystal structure at the Se-site in FeSe superconductor.

Meanwhile, the area of interest is indicated near 50% Se in the phase diagram presented in figure 4.1 with bold partition. This area is of great interest because the superconducting state of FeSe-system occurs within this region. Other parts of this phase diagram does not favor the emergency of superconductivity [29] because of the absence of tetragonal phase of FeSe which shows superconductivity. Among the goals of this research work is to prepare superconducting samples of FeSe in which tetragonal phase is greatly favored and stabilized. In accordance to the phase diagram presented in figure 4.1, FeSe material turns into liquid phase when heated above 1075°C. (not shown). This suggests that any superconducting samples have to be prepared from the liquid close to this temperature, or using solid-state reaction below 1075°C.

Extra care has to be practiced during cooling to prevent phase separation; quenching to low temperatures is necessary to obtain uniform alloy. One of our goals is to establish a way of synthesizing FeSe superconductors in such a manner that the superconducting tetragonal (α -phase) or hexagonal (β -phase) phase is favored and stabilized.

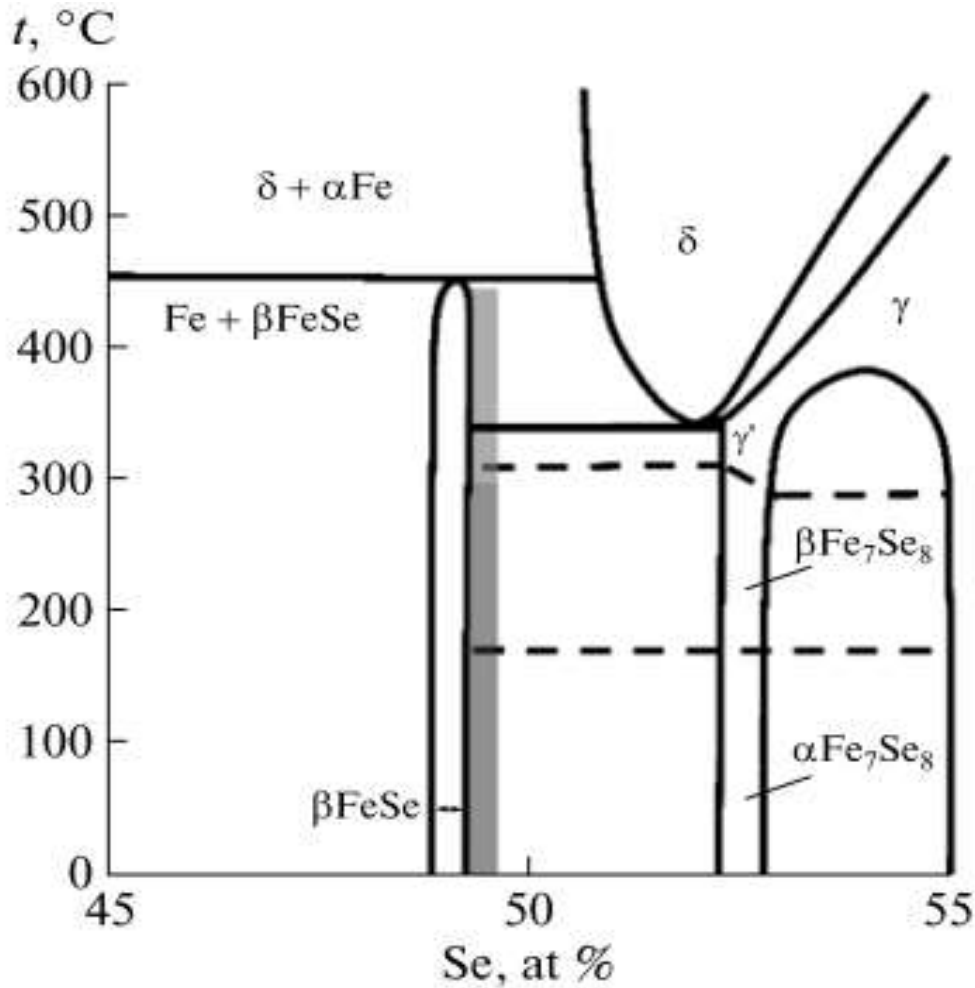


Figure 4.2 The Phase diagram of Fe-Se system[9]

4.1.1 Set Q1 Sample

It is desirable to begin the analysis of the x-ray diffraction with sample that was annealed at very high temperature and quenched from 700°C to the room temperature. Quenching was done

from high temperature to preserve the structural phase attained at 700°C. Figure 4.2 shows the x-ray diffraction pattern of this sample (FeSe) with different plane indices. The structural parameters of this sample are presented in table 4.1.

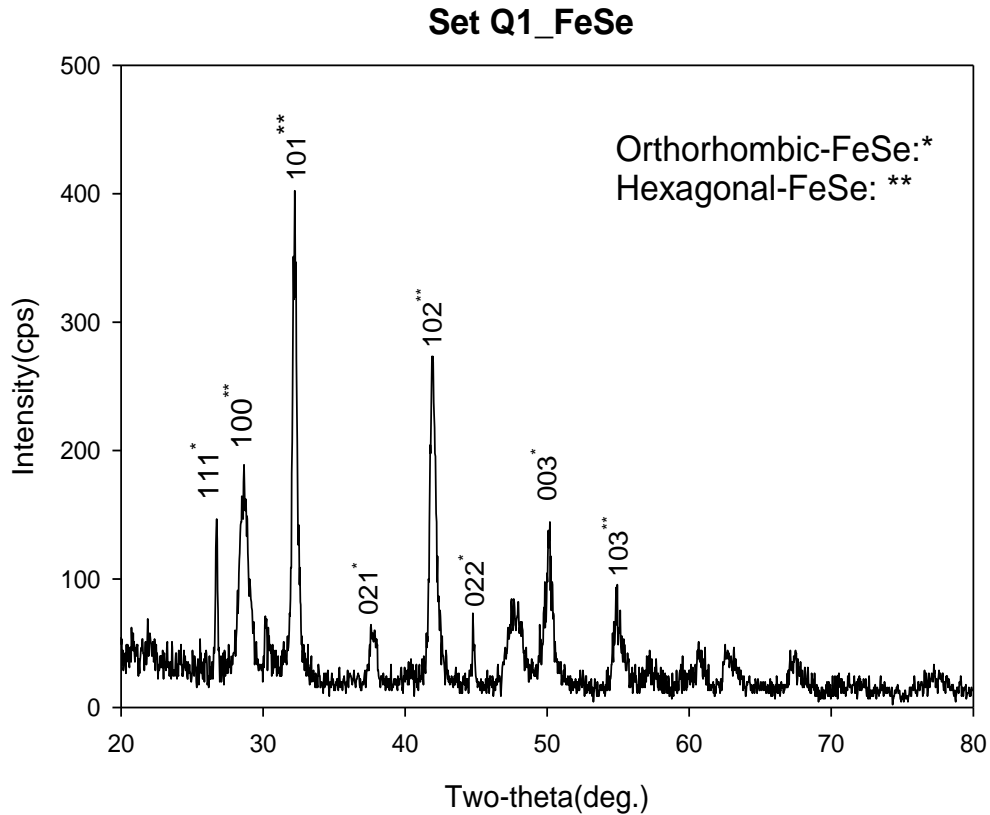


Figure 4. 2: X-ray diffraction pattern of set Q1- FeSe with plane indices

It can be deduced from figure 4.2 that all of the intense peaks come from non-superconducting phase (impurities). The plane indices that correspond to hexagonal non-superconducting phase include (102), (100), (101),(003) and (103) .This result shows that the FeSe sample prepared in this way has high tendency of being non-superconductor because of the fact that the tetragonal shape that enhance superconductivity is not favored. Consequently, the need to anneal the FeSe

sample at relatively low temperature might be needed to promote the tetragonal phase (compare with Q2 samples). The structural parameters for obtained phases are presented in table 4.1a. Table 4.1a also compares our structural parameters with the values obtained from literatures. The comparison shows that our obtained lattice parameters FeSe are very close to the values in the literature.

4.1: Structural parameters of the non- superconducting phase

$a(\text{\AA})$	$b(\text{\AA})$	$c(\text{\AA})$	$V(\text{\AA})^3$	Structure
3.63	3.63	5.91	67.82	Hexagonal
5.28	5.33	5.45	54.04	orthorhombic
5.28	5.29	5.44	76.18	Orthorhombic[26]
4.00	4.00	5.88		Hexagonal[30]

4.1.2 Set Q2 sample

XRD results for Q1 sample suggests that high temperature quenching did not promote the formation of the tetragonal phase, as it does not exist at temperatures higher than 450°C. It is necessary to anneal such a temperature for long time, then quench to room temperature. It is preferable to quench from temperatures lower than 450°C . To enhance the tetragonal (the superconducting) phase of FeSe, the set of samples prepared in this case was not quenched but rather underwent first and second annealing processes. The x-ray pattern of the first member of this set is presented in figure 4.2.

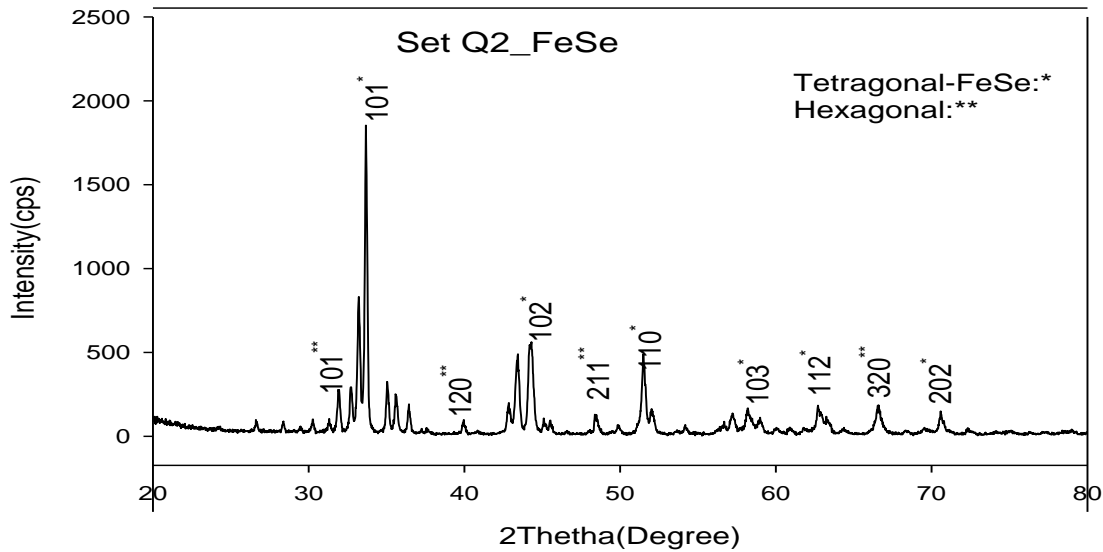


Figure 4. 3: X-ray diffraction pattern of set Q2- FeSe with plane indices

The patterns illustrated in figure 4.3 are quite different from the pattern obtained in figure 4.2 in terms of presence of the superconducting tetragonal phases. Before comparing the intensity as well as the (hkl) indices of the peaks obtained in both cases, it can be clearly seen that the peaks shown in figure 4.3 (Q2 samples) are sharper than what was obtainable in figure 4.2 (Q1 samples). The sharpness of the peaks suggests better crystalline structures and well-formed phase. Furthermore, Q2 sample has less impurity phases than Q1 sample. Comparison of figure 4.2 with figure 4.3 indicates improvement in the superconducting phase at the expense of the impurity phases in samples annealed and quenched from low temperatures (400°C). In addition, the non- superconducting phase represented by plane index (101) in figure 4.2 has changed to superconducting phase in figure 4.3 with improved intensity. High intense peaks from this sample come from tetragonal phase which shows that this method of fabrication (of Q2 samples) promotes tetragonal-FeSe and demotes other non-superconducting phases.

The x-ray diffraction patterns obtained for $\text{FeSe}_{1-x}\text{As}_x$ as the concentration of arsenic increases to 1%, 2%, 4%, 6%, 8% and 10% are shown in Fig 4.4 – Fig 4.9.

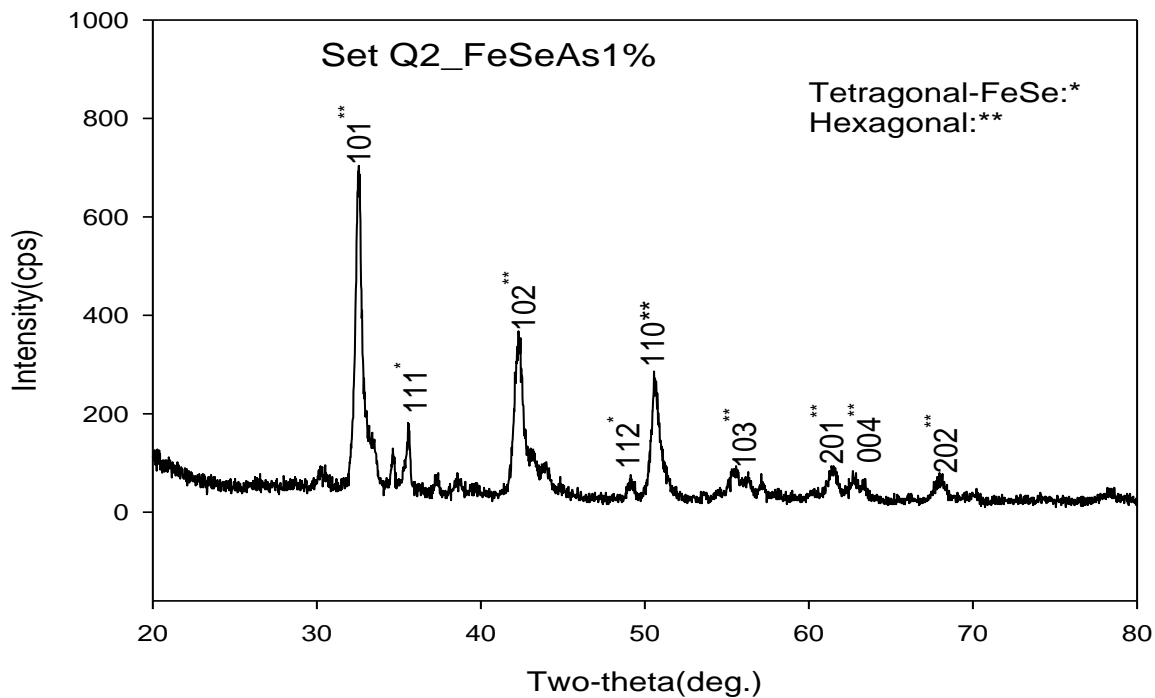


Figure 4. 4: X-ray diffraction pattern of FeSeAs 1% with plane indices

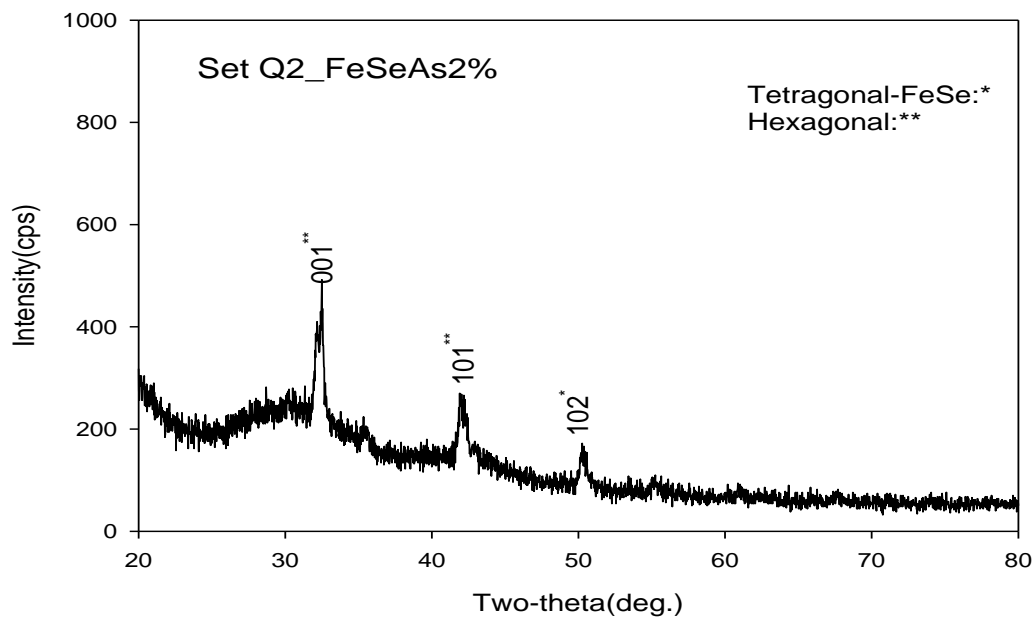


Figure 4. 5: X-ray diffraction pattern of FeSeAs 2% with plane indices

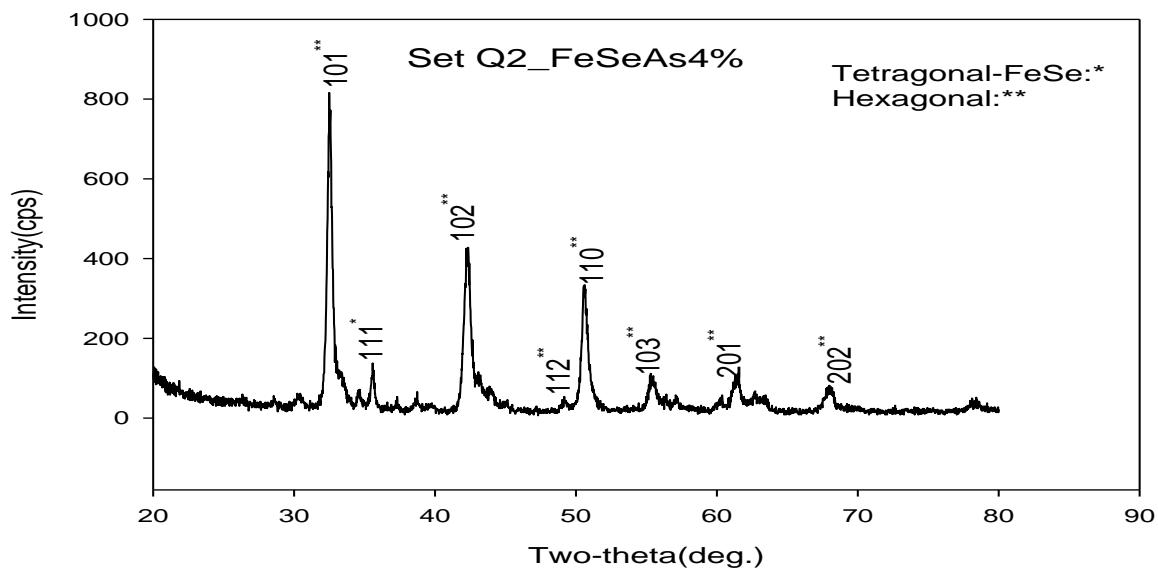


Figure 4. 6: X-ray diffraction pattern of FeSeAs 4% with plane indices

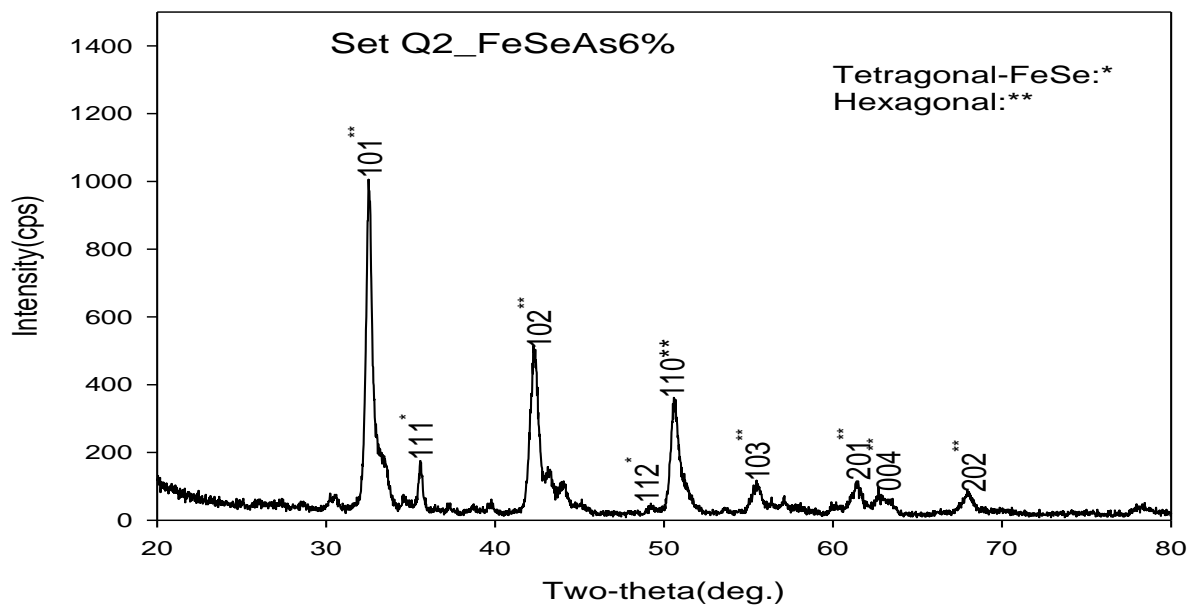


Figure 4. 7: X-ray diffraction pattern of FeSeAs 6% with plane indices

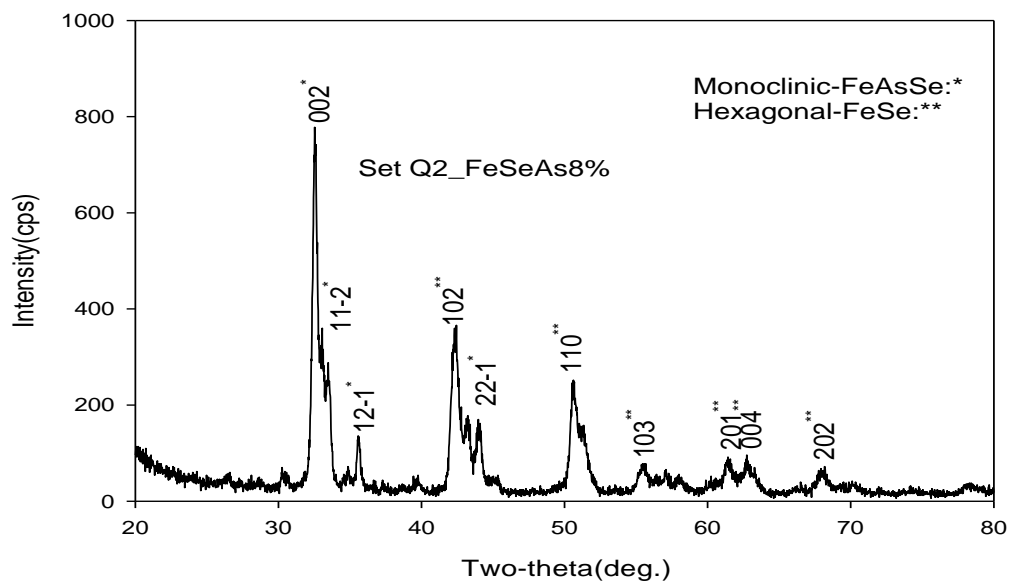


Figure 4. 8: X-ray diffraction pattern of FeSeAs 8% with plane indices

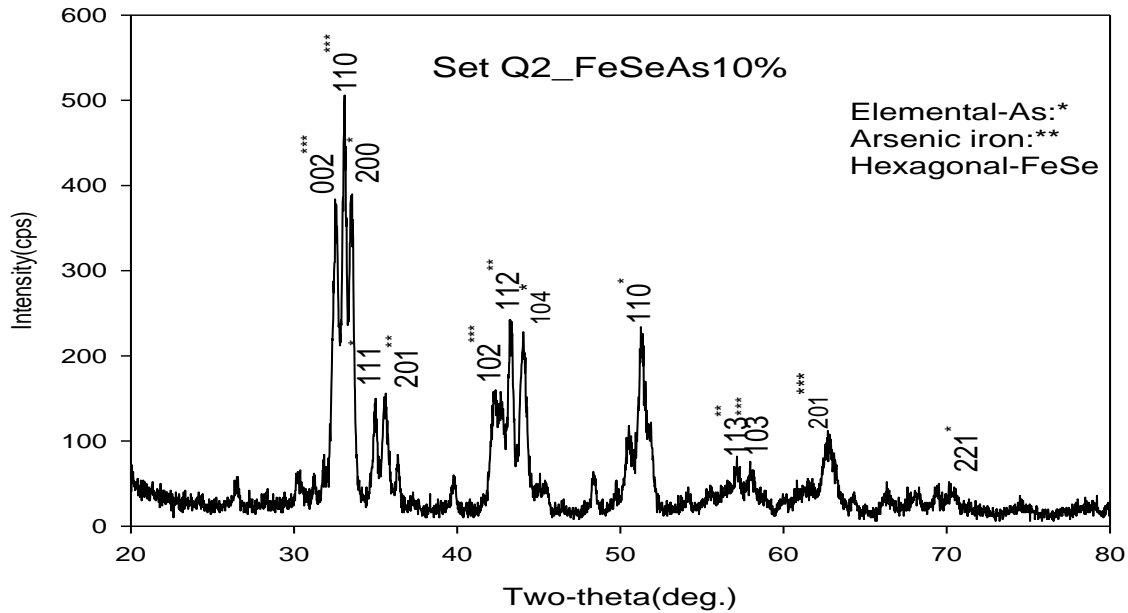


Figure 4. 9: X-ray diffraction pattern of FeSeAs 10% with plane indices

The patterns represented in figure 4.4 to figure 4.9 show the way in which the substitution of arsenic atoms affect the superconducting phase. All figures revealed that the hexagonal phase starts forming with arsenic substitutions. The intensity of the peaks of the tetragonal phase is gradually reduced until the whole phase disappears and the hexagonal phase dominates at the concentration above 6%. The patterns become completely devoid of tetragonal phase at the concentrations above 6% and the material becomes non-superconductors. The variations of the structural lattice parameters with increasing arsenic concentration for both tetragonal and hexagonal phases are represented in table 4.2 (a and b) and figures 4.10 (a and b).

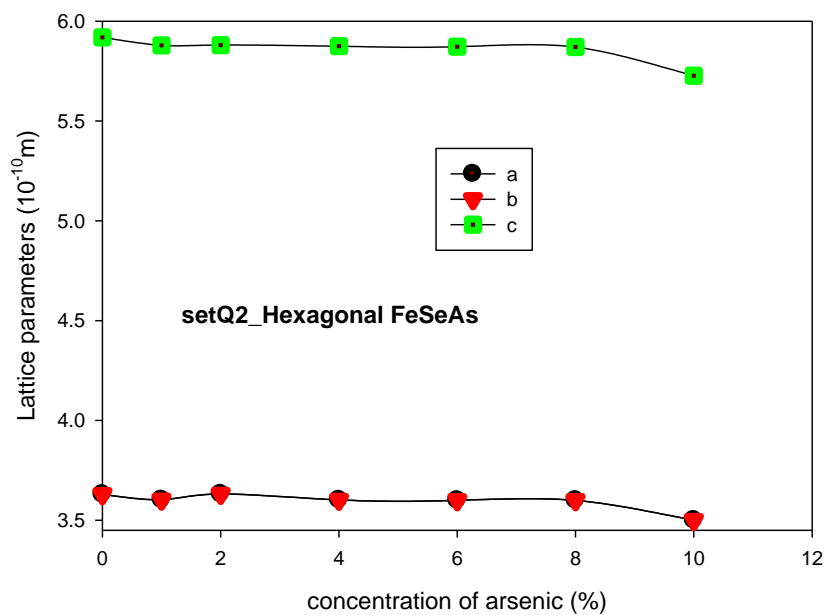


Figure 4.10a: Variation of lattice parameters with the concentration As in setQ2_FeSeAs (Hexagonal)

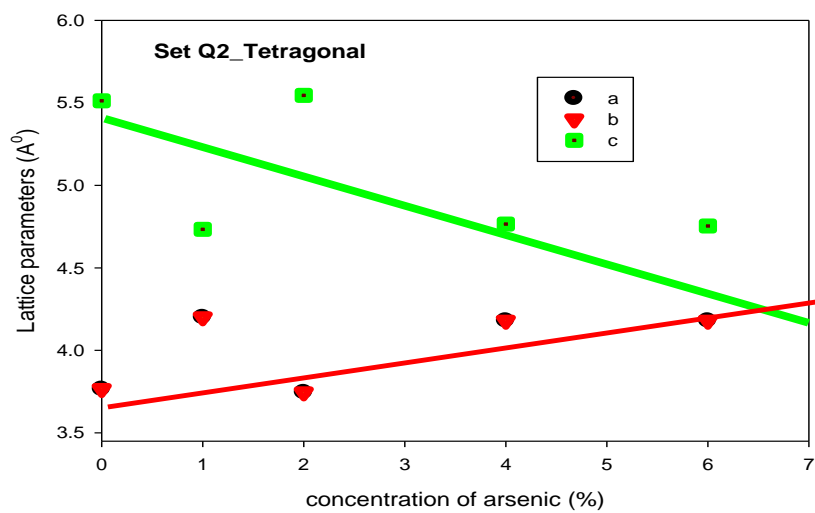


Figure 4.10b: Variation of lattice parameters with the concentration As in set Q2_FeSeAs (Tetragonal)

Figure 4.10(a and b) shows reduction in the lattice parameters as the concentration of arsenic in $\text{FeSe}_{1-x}\text{As}_x$ sample increases. This decrease in the lattice parameter can be accounted for as a result of the fact that the radius of arsenic is smaller than that of selenium. This indicates that arsenic atoms penetrate into the crystal structure of selenium.

Table 4.2: Structural parameters of the superconducting phase of set Q2 samples

% of arsenic	a(Å)	b(Å)	c(Å)	V(Å ³)	Structure	Phase Name
0	3.76	3.76	5.51	78.20	Tetragonal	FeSe
0	3.66	3.66	5.33	71.81	Tetragonal	FeSe[26]
1%	4.20	4.20	4.733	83.54	Tetragonal	FeSe
2%	3.74	3.74	5.54	77.82	Tetragonal	FeSe
4%	4.18	4.18	4.76	83.26	Tetragonal	FeSe
6%	4.18	4.18	4.75	83.05	Tetragonal	FeSe

Table 4.3: Structural parameters of the non- superconducting (impurity) phase of set Q2 samples

% of arsenic	a(Å)	b(Å)	c(Å)	V(Å ³)	Structure	Phase Name
0%	3.63	3.63	5.91	67.56	Hexagonal	FeSe
1%	3.60	3.60	5.87	66.10	Hexagonal	FeSe
2%	3.63	3.63	5.88	67.17	Hexagonal	FeSe
4%	3.60	3.60	5.87	66.00	Hexagonal	FeSe
6%	3.60	3.60	5.87	65.91	Hexagonal	FeSe
8%	3.60	3.60	5.87	65.89	Hexagonal	FeSe
8%	5.96	5.87	6.00	193.80	Monoclinic	FeAsSe
10%	3.50	3.50	5.72	60.77	Hexagonal	FeSe
10%	3.54	3.54	8.92	97.17	Hexagonal	As
10%	5.40	3.30	6.08	108.60	orthorhombic	AsFe

4.1.3 Set Q3 sample

In order to further explore the effect of arsenic on the hexagonal phase formation in FeSe, another set of samples were prepared (preparation procedures are well described in the previous chapter) by quenching from 350°C down to the room temperature.

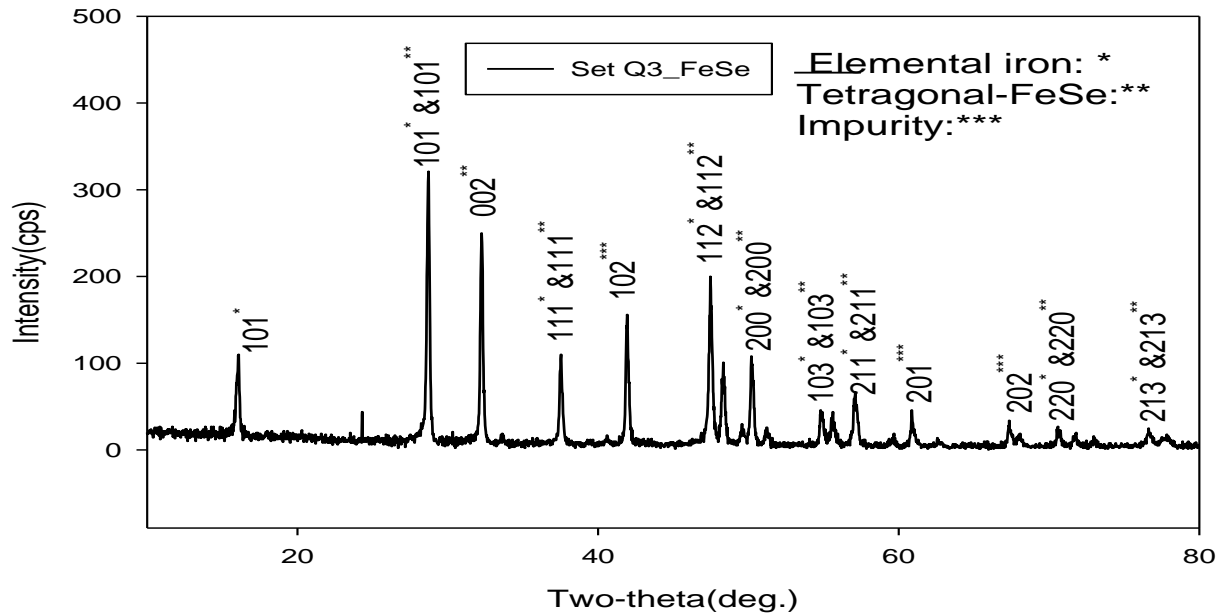


Figure 4.11: X-ray diffraction pattern of FeSe with plane indices

The x-ray diffraction pattern of the un-doped FeSe sample is presented in figure 4.11. The result of the analysis shows three phases which include tetragonal-FeSe, hexagonal-FeSe and elemental iron. Quenching process was mainly carried to minimize the formation of hexagonal phase and promote tetragonal phase which is known to exist above the temperature of 300°C [31].

It is worthy of mentioning that the presence of excess iron helps in stabilizing the tetragonal phase (the superconducting phase). The superconducting tetragonal phases has been investigated either by using excess iron ($\text{Fe}_{1+\delta}\text{Se}$) [31] or deficient selenium ($\text{FeSe}_{1-\delta}$) [33,10].

It seems that the annealing procedure that we follow to prepare FeSe is effective in producing the tetragonal phase. This calls for further investigation and adopt the method to low

concentration of arsenic substituted samples. The results of the x-ray diffraction on the samples with 0.5%, 1% and 3% of arsenic are presented in figures 4.12,4.13 and 4.14

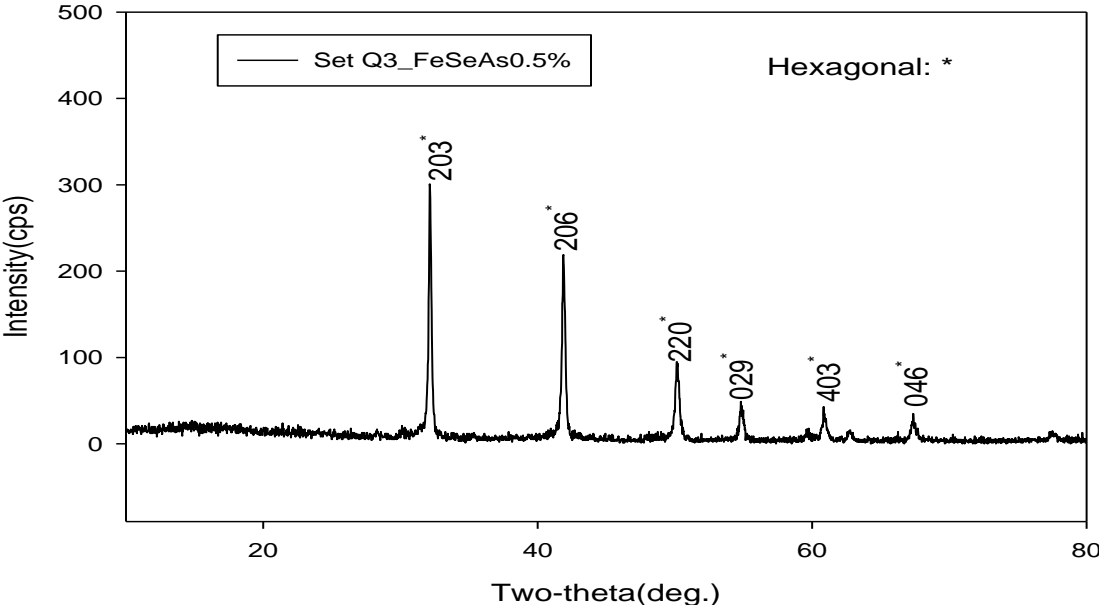


Figure 4.12: X-ray diffraction pattern of FeSeAs 0.5% with plane indices

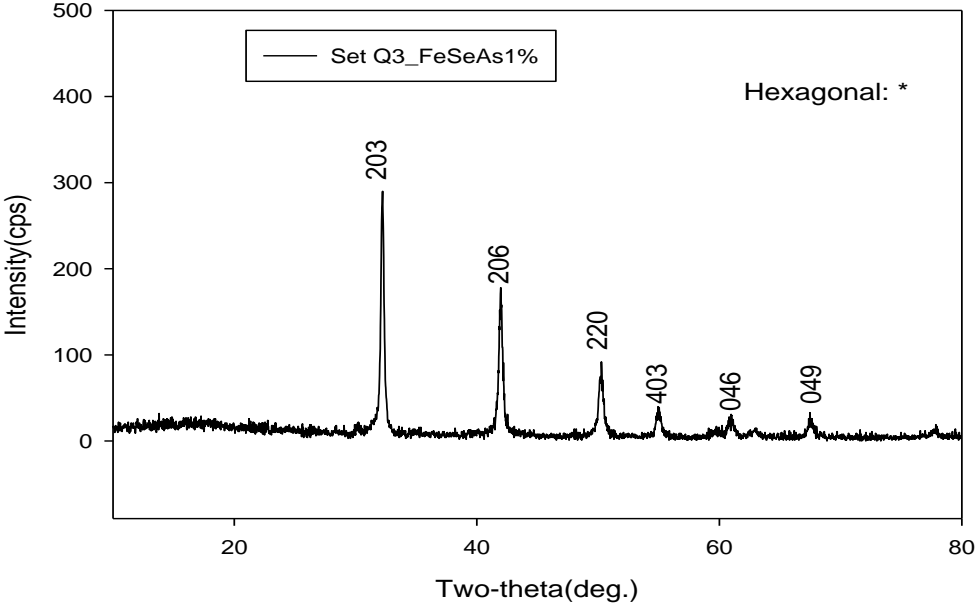


Figure 4.13: X-ray diffraction pattern of FeSeAs 1% with plane indi

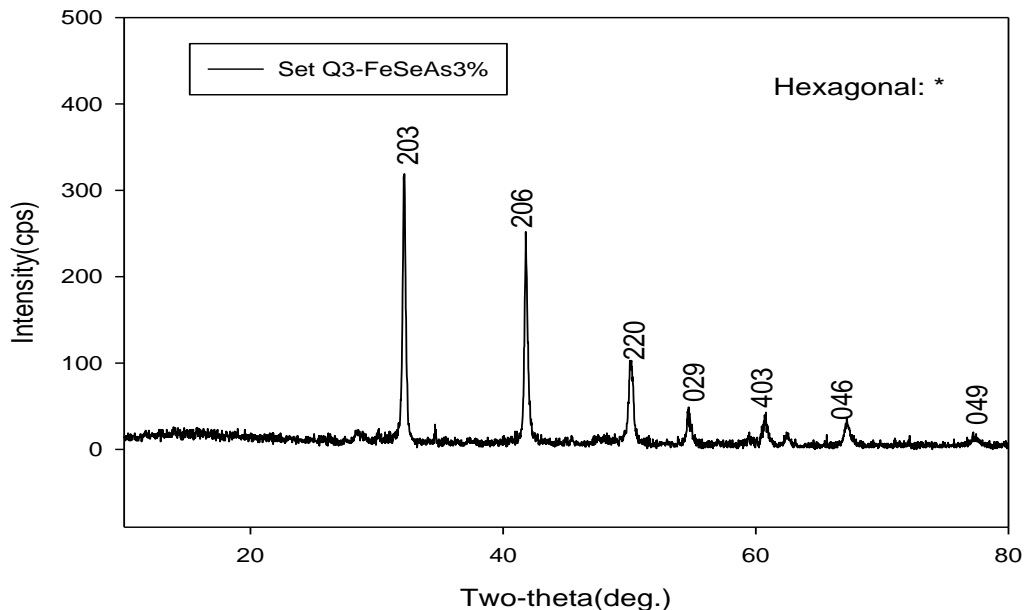


Figure 4.14: X-ray diffraction pattern of FeSeAs 3%with plane indices

These figures (4.12, 4.13 and 4.14) reveal that Fe-impurity phase and the structure is purely hexagonal. The presence of arsenic promotes hexagonal phases. Since iron stabilizes the tetragonal phase of FeSe, the presence of arsenic seems to help better reaction of the constituents. Once the elemental iron particles are completely reacted, the formation of hexagonal phase is being promoted and the structure becomes purely hexagonal. It takes only 0.5% of arsenic to obtain a pure hexagonal phase (Fig. 4.12).

Further increase in the concentration of arsenic brings no significant effect to the system. Similar findings have been revealed from the magnetic measurements and are presented in the following chapter. The lattice parameters and the volume of the unit cell for the tetragonal and hexagonal phases are presented in table 4.4 and 4.4 respectively. The variation of lattice

parameters with the concentration of arsenic in $\text{FeSe}_{1-x}\text{As}_x$ (Hexagonal phase) is presented in figure 4.15. The decrease in the lattice parameters as the concentration of arsenic further explains that the radius of arsenic is smaller than selenium. Hence, the lattice parameters decrease as arsenic gets into the crystal structure of selenium.

Table 4.4: Structural parameters of set Q3 samples

% of arsenic	a(Å)	b(Å)	c(Å)	V(Å ³)	Structure	Phase Name
0	3.76	3.76	5.52	78.42	Tetragonal	FeSe

Table 4.5: Structural parameters of the impurities phase of set Q3 samples

% of arsenic	a(Å)	b(Å)	c(Å)	V(Å ³)	Structure	Phase Name
0	3.63	3.63	5.91	67.56	Hexagonal	FeSe
0	3.76	3.76	5.50	78.18	Hexagonal	Fe
0.5	7.27	7.27	17.75	814.30	Hexagonal	FeSe
1.0	7.25	7.25	17.72	809.01	Hexagonal	FeSe
3.0	7.28	7.28	17.79	817.37	Hexagonal	FeSe

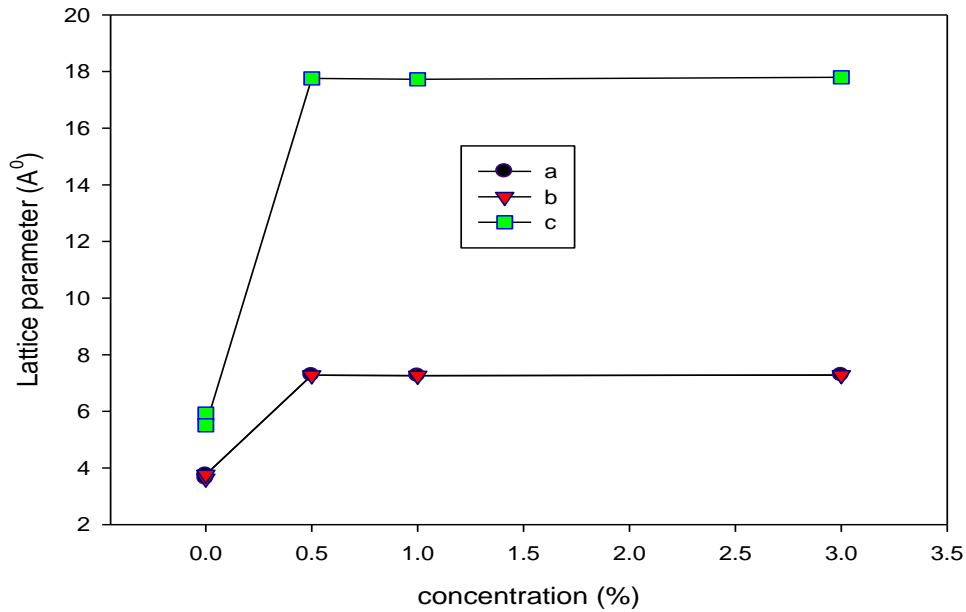


Figure 4.15: Variation of lattice parameters with the concentration As in set Q3_FeSeAs (Hexagonal)

4.2 Transport Measurement

Although our best samples are the set Q3 with pure single hexagonal phase, we could not prepare them in solid bar-shape for resistivity measurement because of being in powder form. However, magnetic measurements were performed on them along with other samples.

Resistivity measurements performed on FeSe $1-x$ superconductor by Margadonna *et al* [10]. They observed an inflection points in the resistivity versus temperature curves. They associated this behavior with tetragonal to orthorhombic structural phase transition at the inflection point [10]. Moreover, Margadonna *et al.* [10], obtained the XRD-patterns for FeSe superconductor at various temperatures (300-4 K) and obtained the variations of the lattice parameters with

temperatures; their results are shown in Fig.4.16. Figure 4.16 [10], shows that both lattice parameters a and b have the same value in(tetragonal phase) diverges as the sample was cooled below 70 K. This temperature marks the structural transformation from tetragonal to orthorhombic phase at low temperatures.

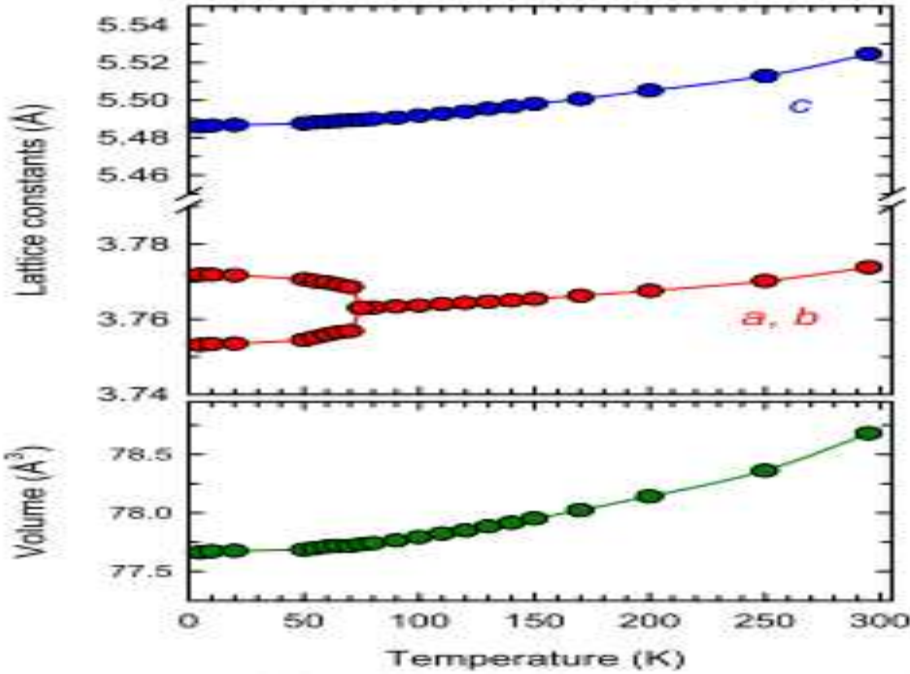


Figure 4.16: Structural transition(from tetragonal to orthorhombic) observed in FeSe superconductor [10]

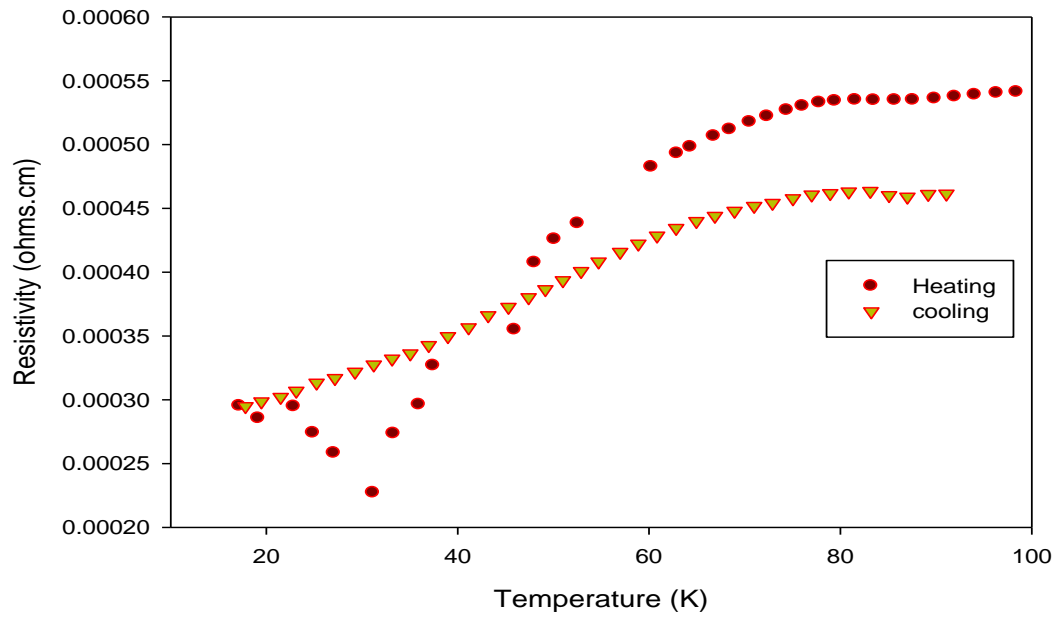


Figure 4.17: Transport measurement for set Q2_FeSe

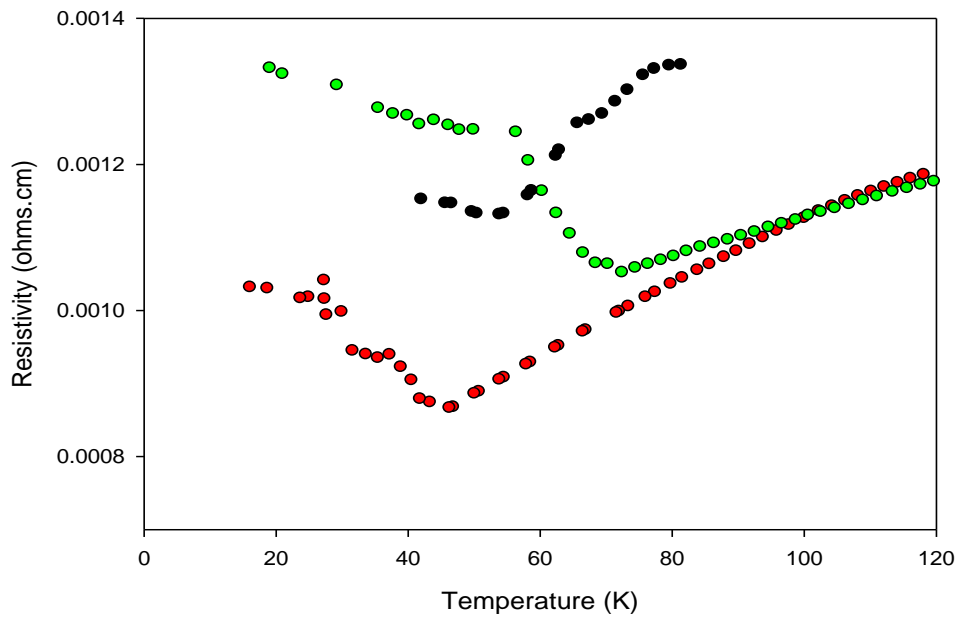


Figure 4.18: Low temperature comparison of the structural transition in superconducting samples of Set Q2

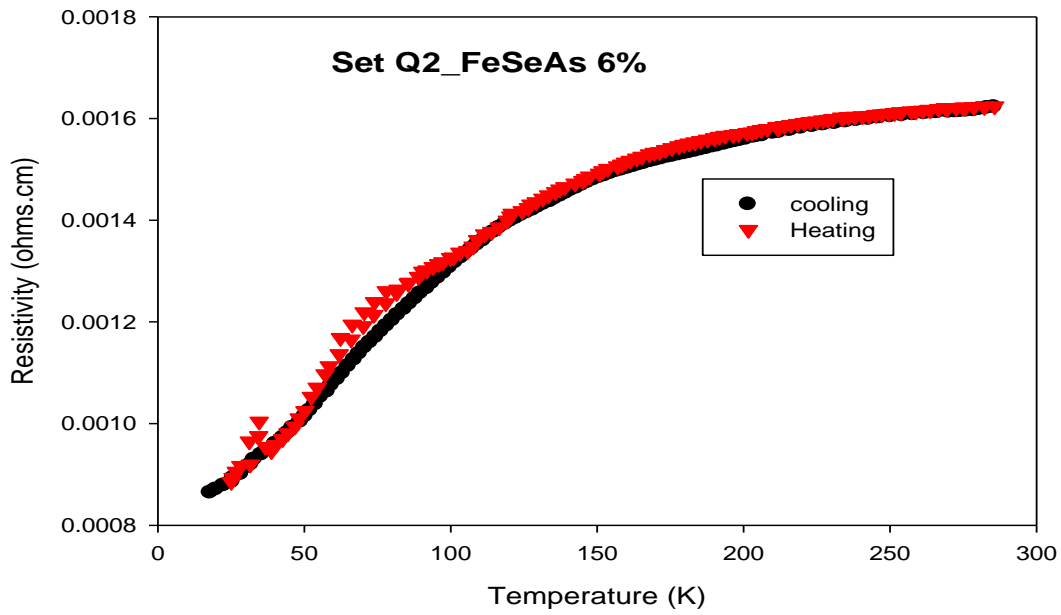


Figure 4.19: Transport measurement for set Q2_FeSeAs 6%

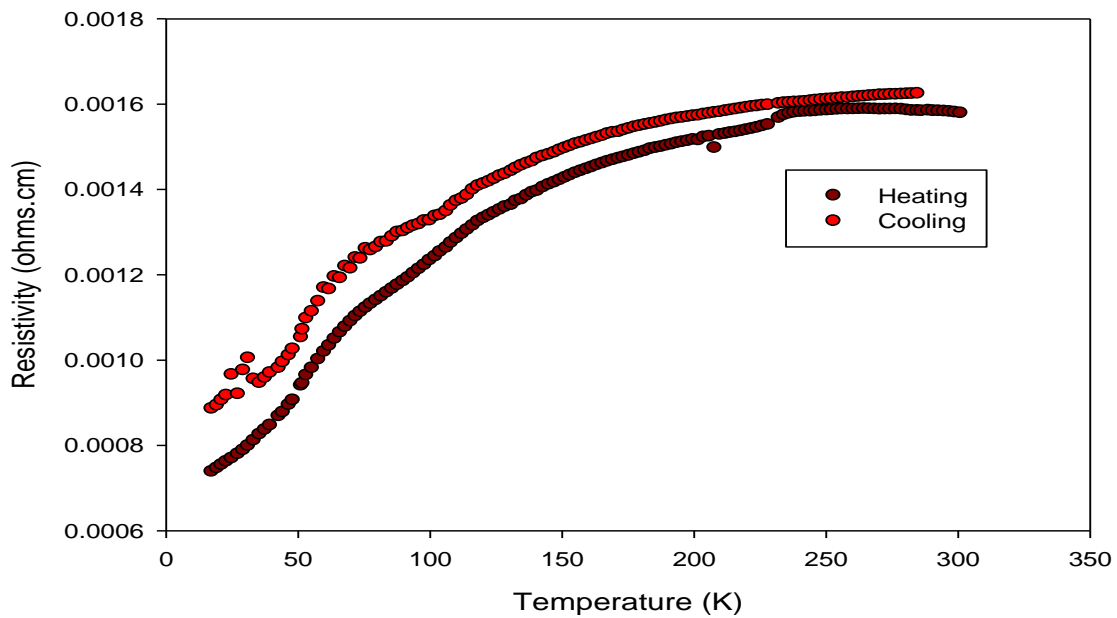


Figure 4.20: Transport measurement for set Q2_FeSeAs 8%

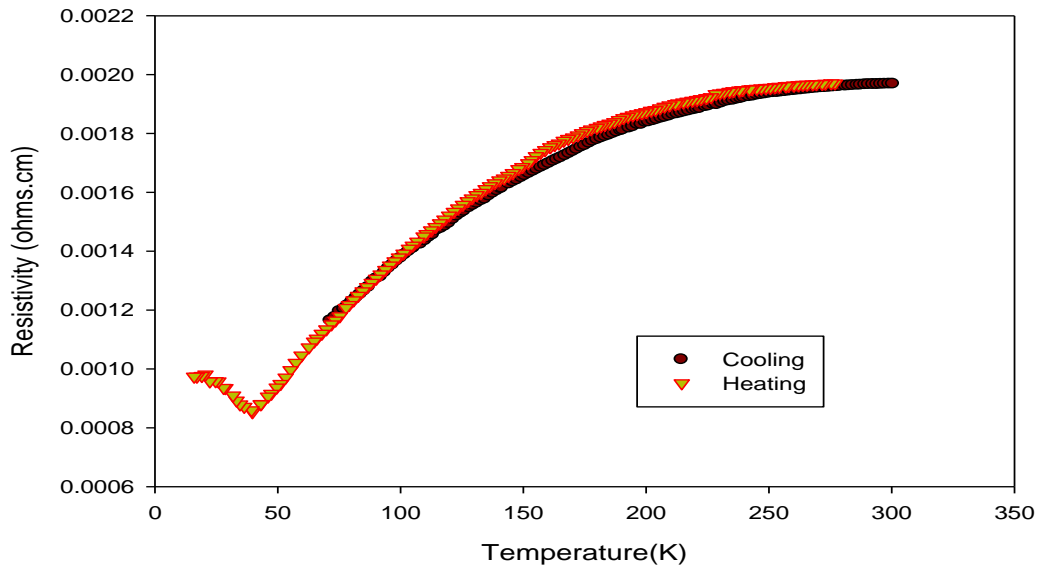


Figure 4.21: Transport measurement for set Q2-FeSeAs 10%

Figure 4.17 to figure 4.21 show the result of the transport measurement conducted on set Q2 samples. The measurements were conducted during cooling and heating of the concerned samples in the temperature range (300 -14) K.

The figures revealed that the resistivity decreases as the samples were cooled down to low temperature (14 K) Moreover; the graphs obtained during the resistivity measurements show points of inflection which were more pronounced during heating measurements

Similarly, this kind of behavior is observed in the resistivity measurements performed in our samples. Figures 4.17 to 4.21 show points of inflection around a temperature below 100 K. These observed structural transitions in our prepared samples can be easily accessed and understood from a graph of the derivative of the resistivity with temperature against temperature. Observation of an isolated extremum at a point along the temperature axis signifies a point of inflection in a graph of the derivative of the resistivity with temperature against

temperature. This inflection point corresponds to a significant change in the slope, from concave to convex or vice versa.

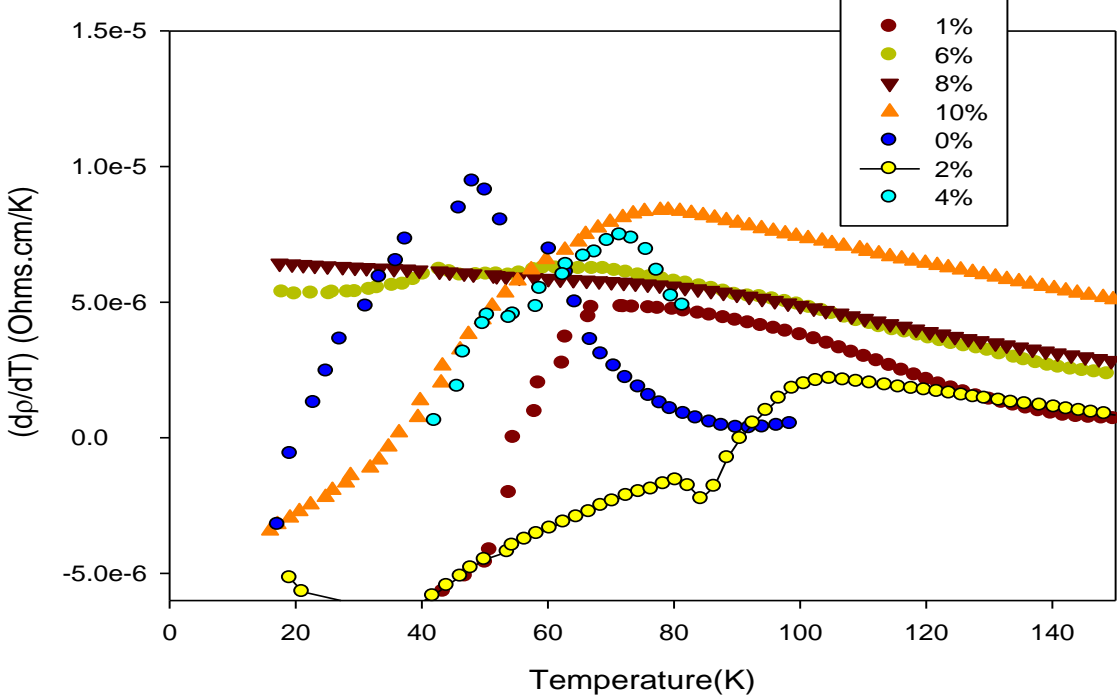


Figure 4.22: Derivation of the resistivity with temperature

A graph of the derivatives of resistivity with temperature is depicted in figure 4.22. The temperature corresponds to the maximum point indicates the actual temperature at which the structural transition occurs. These structural transition temperatures for all the samples are presented in table 4.5. Meanwhile, these values will be of guide while constructing a phase diagram of Fe(Se,As) system.

Table 4.5: Structural transition temperature with concentration of arsenic for set Q2 samples

Concentration of arsenic (%)	Structural transition Temperature (K)
0	48.04
1	71.83
2	104.69
4	71.43
6	63.00
8	79.53
10	78.43

4.3 Variation of magnetization with temperature for set Q2 samples

The trend of the magnetic moment with temperature is depicted in figure 4.23 and 4.24 for different concentrations of arsenic. The observed sudden change in slope commensurate the report in the literature [15]. The points of inflection associated with magnetic –temperature measurement results from magnetic anomaly which could be attributed to rearrangement of spins [15]. For the effective visualization of the similitude of magnetic transition reported in the literature for FeSe superconductor [15], differentiations of the results of magnetic moment

with respect to temperature were carried out. The derivatives of the magnetic moment reveal extremum at the point of inflection. In this wise, the graph of the derivatives of the magnetic moment with respect to temperature is presented in figure 4.24. There is no conspicuous inflection in the zero concentration of arsenic while other concentrations show maximum points that correspond to rearrangement of magnetic spins at different temperatures. The temperatures at which the magnetic transitions were observed are presented in table 4.6

Table 4.6: Magnetic transition temperature with concentration of arsenic for set Q2 samples

Concentration of arsenic (%)	Magnetic transition temperature(K)
0	Null
1	112.34
2	127.14
4	129.73
6	129.37
8	130.56
10	131.46

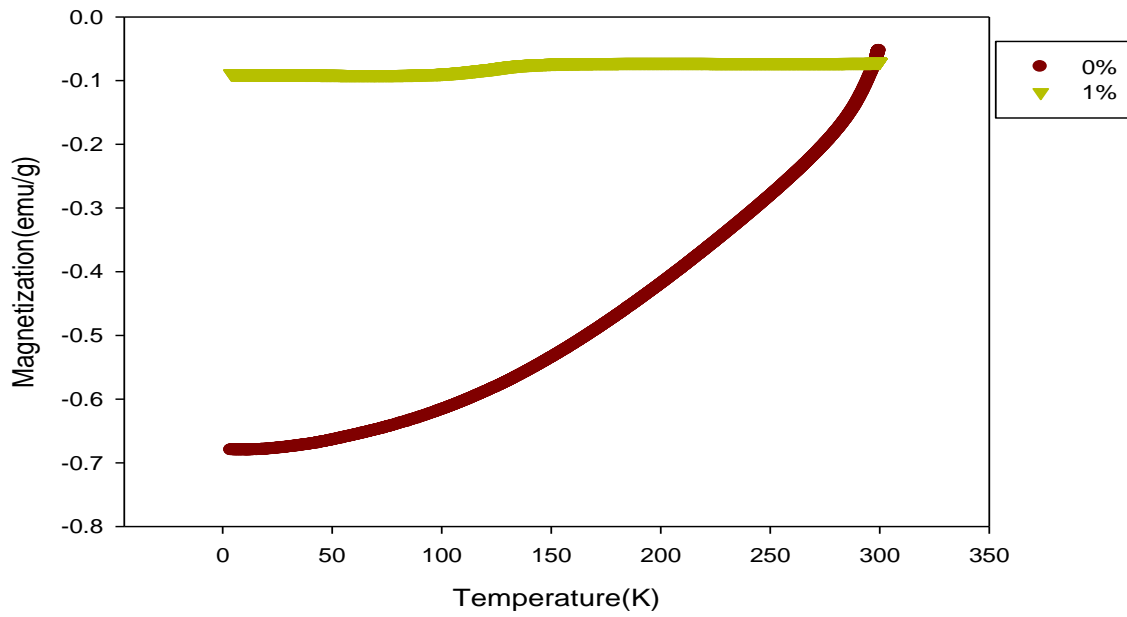


Figure 4. 23: Magnetization dependent temperature for set Q2 samples(0%&1%)

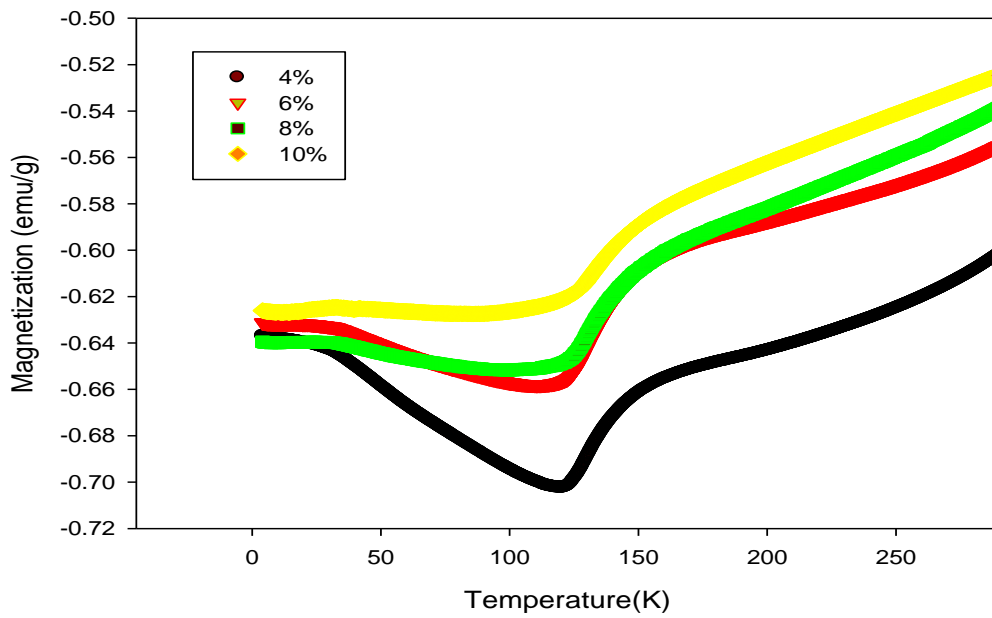


Figure 4. 24: Magnetization dependent temperature for set Q2 samples

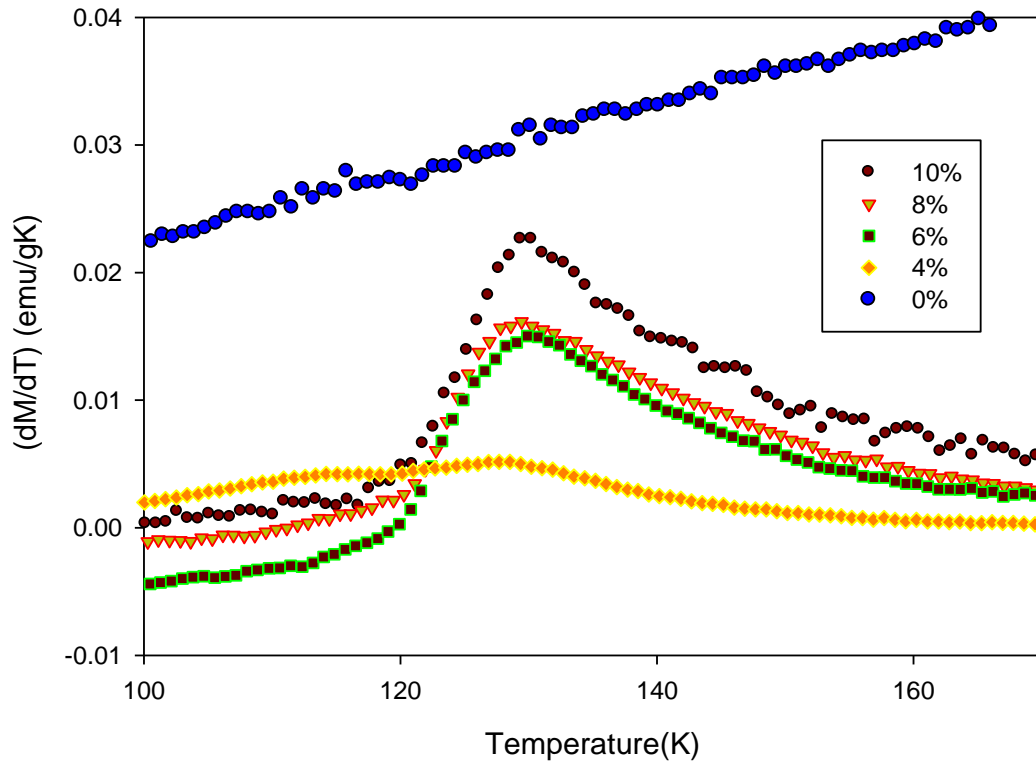


Figure 4. 25: Variation of magnetic moment with temperature

The structural and magnetic transitions, coupled with the observed superconducting transitions (that would be further discussed in from the hysteresis loop) are summarized in the developed phase diagram depicted in figure 4.26. The illustrated phase diagram explains the various transitions that occur in set Q2-FeSeAs system. At temperature below 10 K, the material maintains superconducting state and turns to non-superconductor at temperature above 12 K. Furthermore, structural transitions occur as the material is cooled down below 70 K. This transition occurs between tetragonal to orthorhombic shapes and the material super-conducts in orthorhombic form.

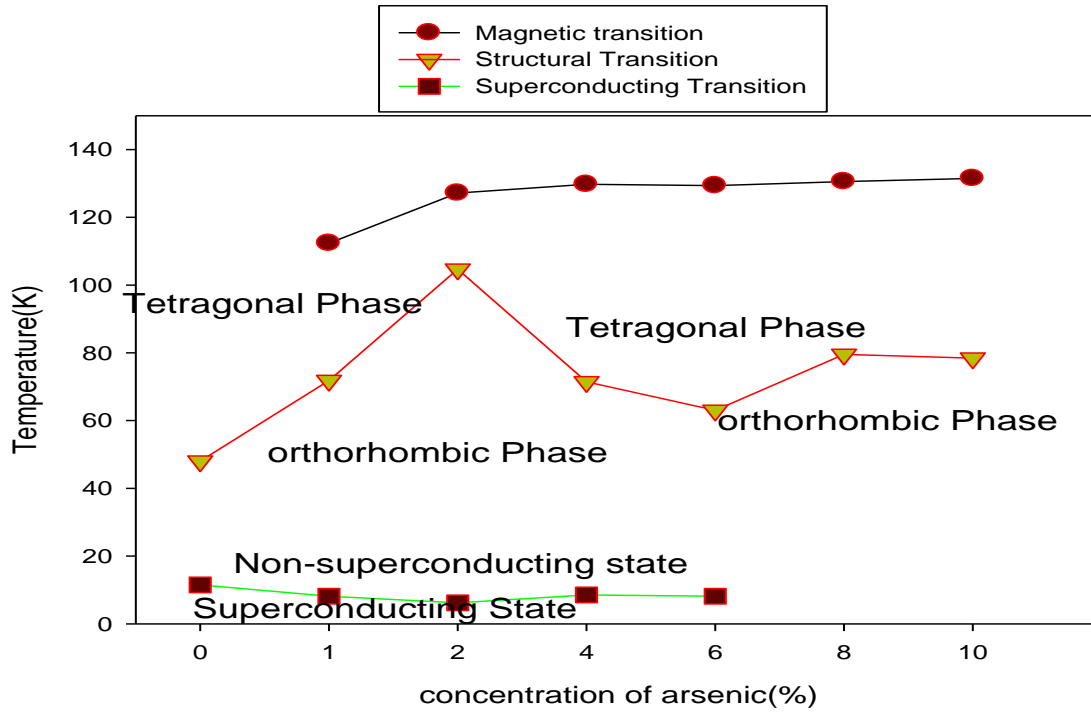


Figure 4. 26: Phase diagram of FeSeAs-system

The description of magnetic transition is not left out in our presented phase diagram.

CHAPTER 5

Magnetic Measurement

Important transitions observed in FeSe superconductor are mainly revealed in its magnetic measurement. Features of the magnetization-temperature graphs of this material have been reported to include a bump and step at temperature around 90 K and 120 K respectively [32]. The observed bump and step were attributed to structural (tetragonal to orthorhombic) and magnetic (anti-ferromagnetic type) transition. These transitions were also observed in our fabricated samples and the details of the transitions are depicted in our developed phase diagram.

5.1 Temperature dependent of magnetic susceptibility for set Q3 sample

For the purpose of proper investigations of the effect of arsenic on $\text{FeSe}_{1-x}\text{As}_x$, magnetic measurement was performed on setQ3 samples which are of lower concentrations of arsenic. The graph of susceptibility against temperature for set Q3 samples is presented in figure 5.1. The zero field cooling (ZFC) and field cooling (FC) for 0% concentration of arsenic demonstrate superconductivity for their respective values of onset temperatures which are 11.5 K and 10.7 K respectively. However, the small substitution of selenium by arsenic returns the sample to pure hexagonal FeSe.

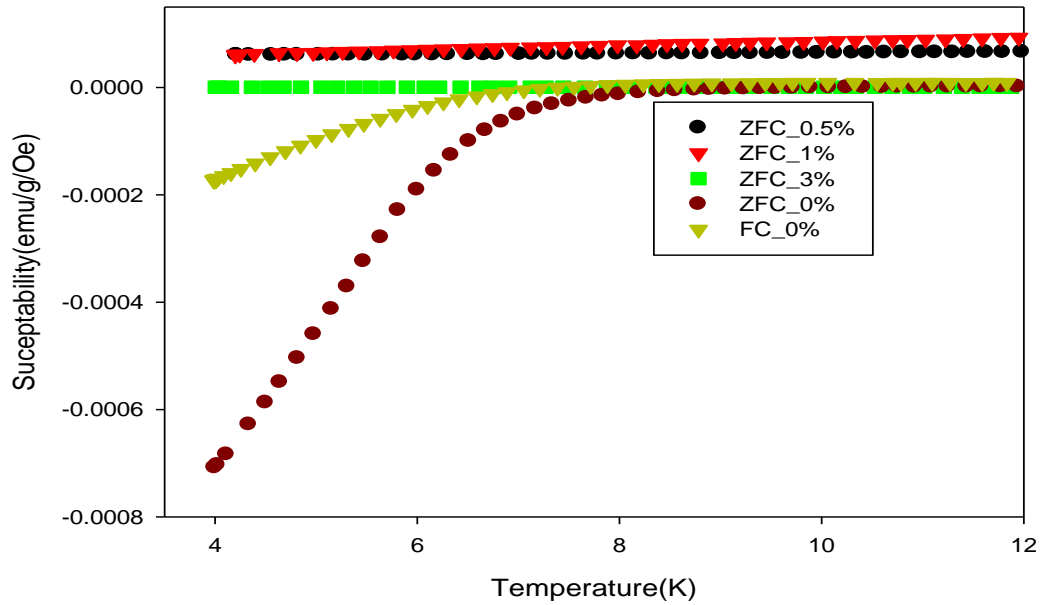


Figure 5.1: Temperature dependent of magnetic susceptibility for Set Q3 samples

Figure 5.1 further reveals that the substitution of 0.5% of arsenic turns the material to pure hexagonal FeSe and the subsequent increase in the concentration make the material to persist in its pure phase.

5.2 Magnetic properties

The variation of the magnetization with the applied magnetic field for Q2 samples $\text{FeSe}_{1-x}\text{As}_x$ with $x = 0.0, 0.01, 0.04$ and 0.06 at 4 K are shown in figure 5.2.

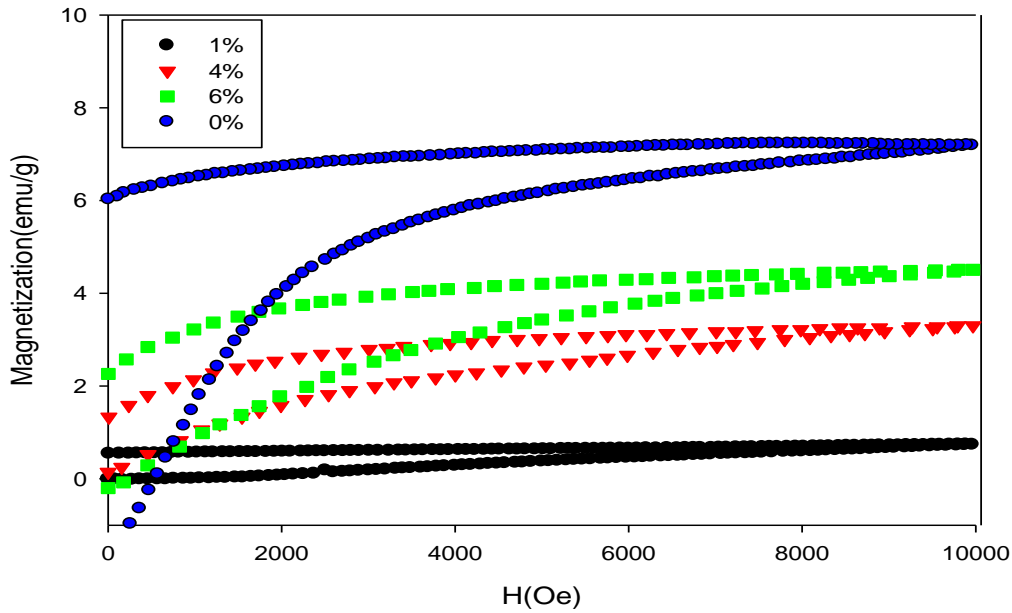


Figure 5. 2: Magnetization against applied field for Set Q2_FeSeAs at 4 K

For all samples with arsenic concentration less than or equal to 6%, the initial magnetization starts with negative slope indicating diamagnetic superconducting state, with strongest signal in sample with zero arsenic content. Increasing the arsenic content increases the saturated magnetization and enhancing the remnant magnetization. The hysteresis loops for samples with higher arsenic contents are similar to Fe, indicating ferromagnetic-like ferromagnetic hysteresis loops. In such a case the contribution to the magnetization from the superconducting phase cannot be separated from the ferromagnetic contribution. This may indicate the presence of both phases at low temperatures (below T_C).

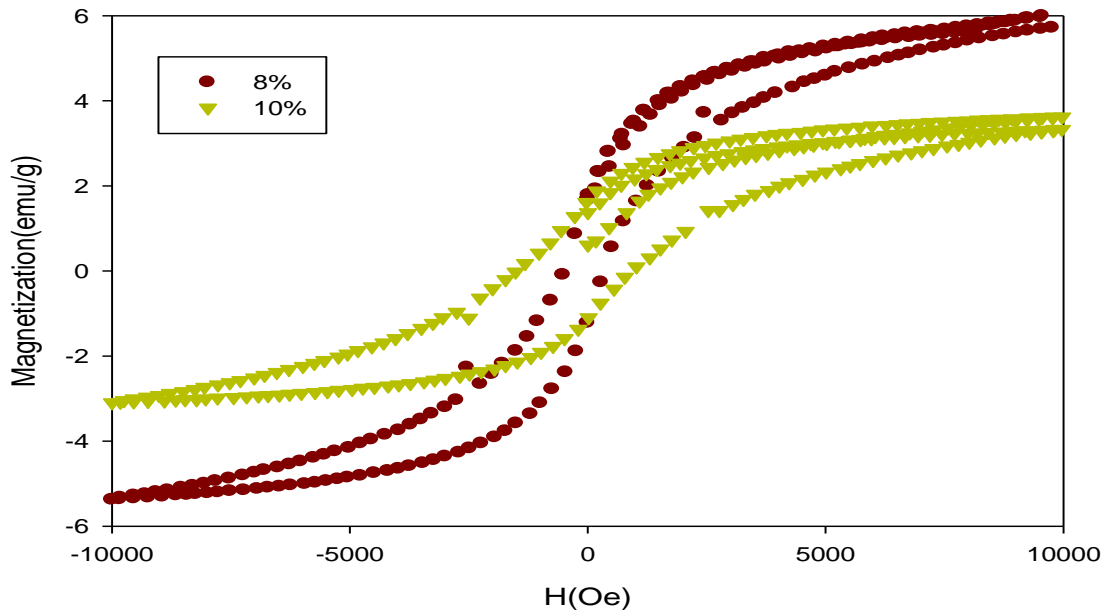


Figure 5. 3: Magnetization against applied field for Set Q2_FeSeAs at 8 K

Figure 5.3 represents the magnetization data for the sample with 8% and 10% arsenic which is completely in a ferromagnetic-like state above 4.2 K. The hysteresis losses decrease with increasing temperature. This is associated with reduction in the saturated magnetization; however with little changes in the remnant magnetization. Since the initial magnetization starts with positive slope for both samples, this may indicate the absence of the superconducting state in these samples. However, it should be mentioned that these samples (with 8% and 10% arsenic) are not single-phase samples.

5.3 The critical current density

The critical current density refers to the maximum current the superconductor can sustain in its superconducting state. Above this critical value the superconducting state is destroyed and the material becomes normal conductor [33]. Critical current density is very important for practical

applications of superconductivity that requires the use and generation of high magnetic fields. The critical current can be measured using transport measurement technique (voltage vs. current), or can be estimated from magnetization measurements using Bean model presented in equation (2). Among the well-known approximate methods of estimating critical current density include the Bean's critical state model [34].

$$J_c = 17 \frac{\Delta M}{R} \quad (2)$$

Where $\Delta M = M^+ - M^-$

M^+ =Increasing field magnetization density

M^- =Decreasing field magnetization density

R= Average radius of the grain size or the sample perpendicular to the applied field.

Bean's critical state model has been used extensively in conventional and non-conventional superconductors to estimate the variations of the critical current density with the applied field [35]. However, it should be noted that Bean's model is applicable for magnetic fields that are larger than the penetration field. According to this model, the critical current density is proportional to the width of the hysteresis loops (ΔM) of the superconducting state.

In figure 5.4 we present the variation of the width of the hysteresis loops ($J_c \propto \Delta M$) (equivalently, the critical current density) with the applied field for Q2-FeSe superconducting sample at 4, 6 and 8 K. The critical current density at different temperature falls rapidly at first and then follows more gradual reduction with increasing field. Three different regions in graph have reported in the literatures [33]. These regions can be understood by assuming that the superconductor possesses several grains amalgamated by weak links.

The initial value of ΔM (at $H = 0$ Oe) is 7.5 emu/g, 7emu/g and 4emu/g at $T = 4, 6$ and 8 K respectively. These values equal twice the remnant magnetization at the corresponding temperatures.

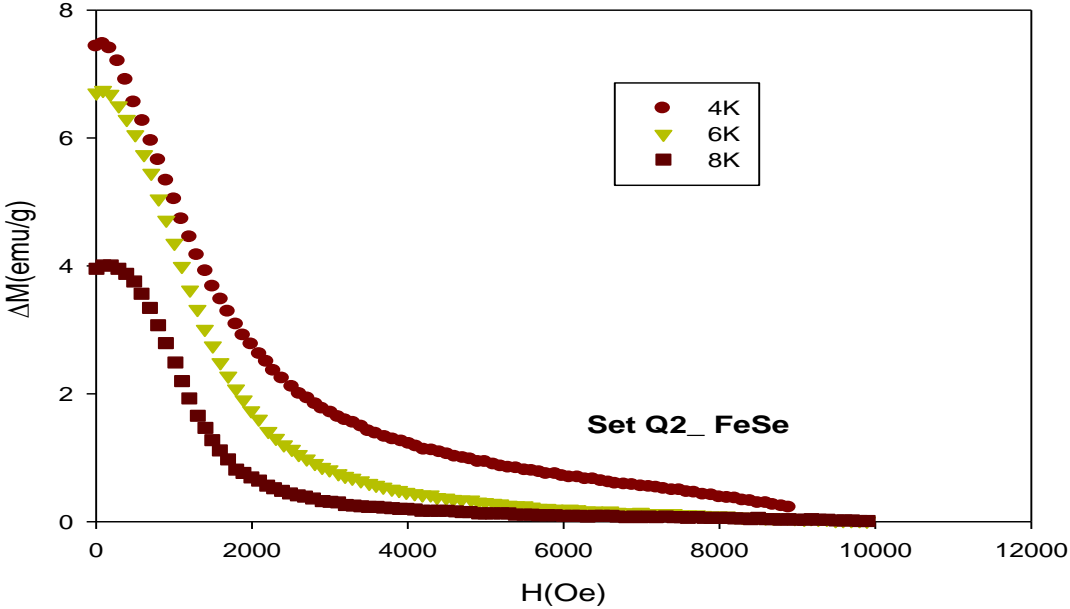


Figure 5. 4: Description of the critical current density at different temperature for set Q2_FeSeAs for 0%As

A gradual increase in the applied field weakens the weak links that join the grains together, thereby rapidly reducing the value of the critical current density at low field [33]. As the value of the applied field is progressively increasing, the critical current density carried by each grains suffer a gradual reduction because of the strong strength which makes the intermediate regime to be linear and occur slowly [33]. The values of the critical current density asymptotically approaches zero at high magnetic field. The value of the applied field at which the critical

current becomes zero is called irreversible field which marks the field at which the flux can no more be pinned and the material automatically becomes non-superconductor. The zero magnetization depends actually on the resolution of the magnetometer used in measuring the magnetization. In our measurements; the magnetization is considered to be zero it drops below 10^{-5} emu, which is the noise level in our magnetometer.

The effect of arsenic in $\text{FeSe}_{1-x}\text{As}_x$ samples ($x = 0.01$ and 0.06) is illustrated in figure 5.5 and 5.6 at temperature of 4 K and 6 K.

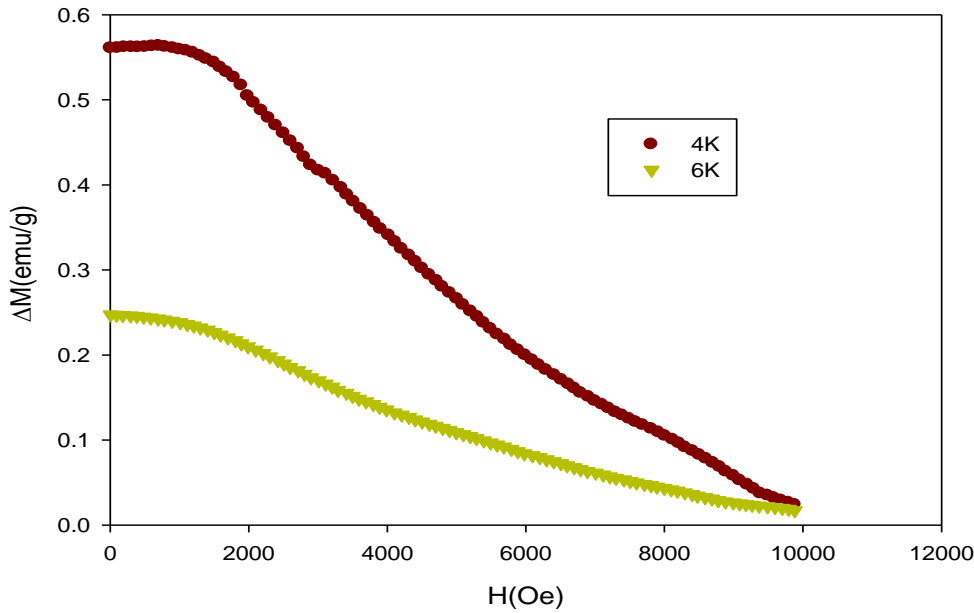


Figure 5. 5: Description of the critical current density at different temperature for set Q2-FeSeAs for 1%As

The arsenic substitution for selenium in FeSe systems shows a drastic reduction of the initial width of the hysteresis loops ΔM (proportional to the critical current density) from 7.5 emu/g to about 0.57 emu/g for 1% concentration of arsenic as shown in figure 5.5. Further reduction in this value was also recorded at 6 K. However, the reduction in ΔM with increasing field is much

slower than what we observed in FeSe sample. This indicates that arsenic substitution is affecting the grains and the critical current associated with these grains. Moreover, an arsenic substitution is enhancing the coupling between the grains.

The variation of critical current at a concentration above which the superconductivity is lost is represented in figure 5.6. At this concentration, the addition of arsenic to FeSe system raises the initial critical current density to around 2.7emu/g and 1.35emu/g at 4 K and 6 K respectively as illustrated by figure 5.6.

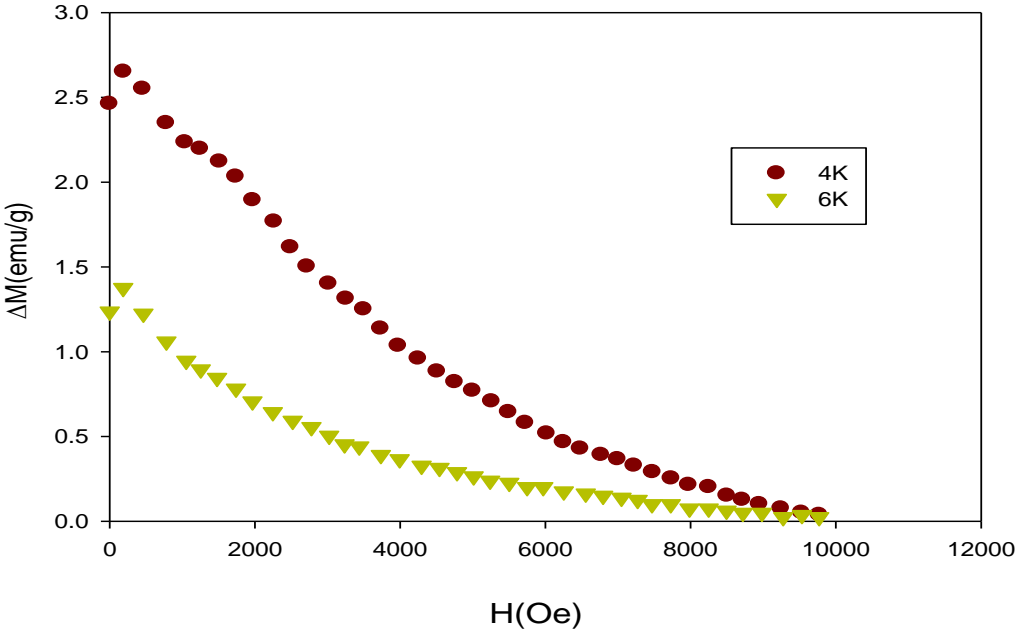


Figure 5. 6: Description of the critical current density at different temperature for set Q2-FeSeAs for 6%As

For the purpose of observing the overall effects of arsenic on all superconducting concentration, figure 5.7 shows the trend of the critical current density for 0%, 1%, 2%, 4% and 6% concentration of arsenic at 4 K.

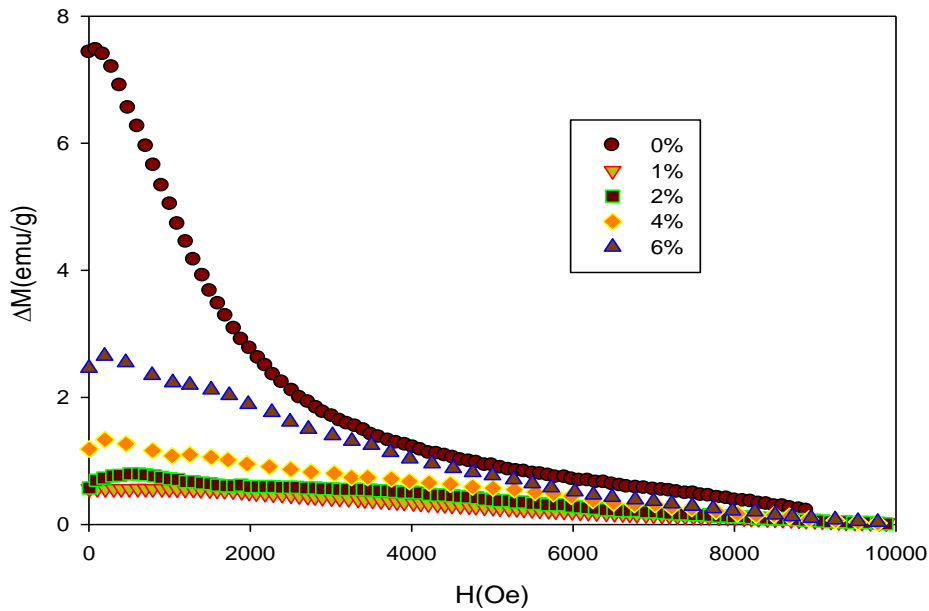


Figure 5. 7: The trend of the variation of critical current density for Set Q2-FeSeAs system at 4 K

The variations of the width of the hysteresis loops at 4 K for FeSe_{1-x}As_x Q2-samples are presented in the figure 5.7. The figure reveals a sudden reduction in the value of the critical current density (ΔM) at the lowest concentration of arsenic ($x = 0.01$). The critical current density further increases with the concentration of arsenic.

5.4 Pinning forces

The pinning centers are the consequences of imperfections in superconductors [36]. These centers that pin the magnetic vortices results from dislocations, defects, domain boundaries to mention but few. Really, these imperfections are of critical significance as it helps the value of critical current to rise. The dependence of the pinning force on the magnetic field is somewhat significant as it reveals the field at which the flux leaves the pinning trap and the material becomes non-superconductor. The knowledge of the pinning force is well comprehended when

we view superconductors as material that have normal cores through which imperfections in meissner effects prevail. The super-current is imagined flowing across these normal cores and the normal cores dominate the material when it turns to non-superconducting state [33].

Just below the lower critical field of type-II superconductor under the consideration, the applied magnetic field is able to penetrate the normal cores which are circumscribed by the super-current. As the field keeps increasing, the normal cores become closely packed so that the vortices feel a kind of force due to the flow of current. The material loses its superconductivity when the force experienced by the vortices due to the flow of current is larger than the pinning force. Subsequently, the material becomes non-superconducting.

The variation of pinning forces for different concentration of arsenic at different temperatures is illustrated in figure 5.8, 5.9, 5.10 and 5.11.

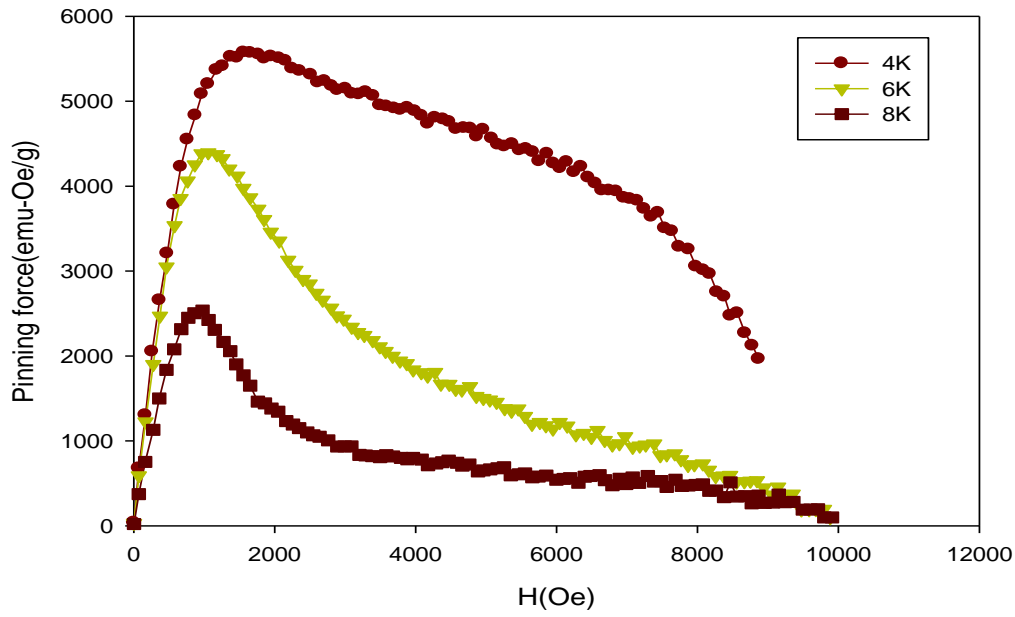


Figure 5. 8: Variation of the pinning force with the applied field for set Q2-FeSe

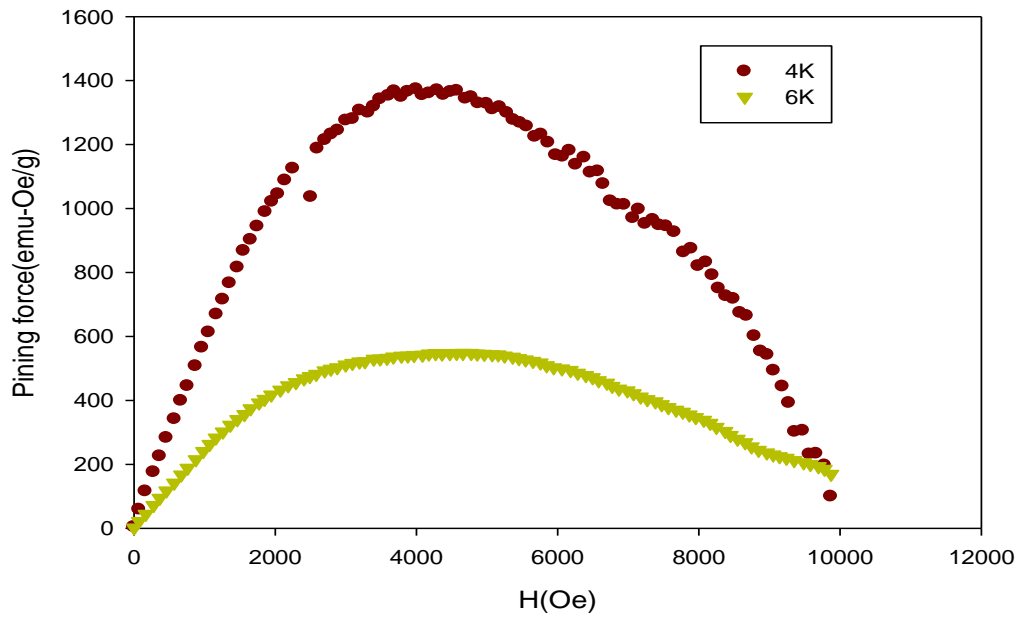


Figure 5. 9: Variation of the pinning force with the applied field for set Q2_FeSeAs 1% of As

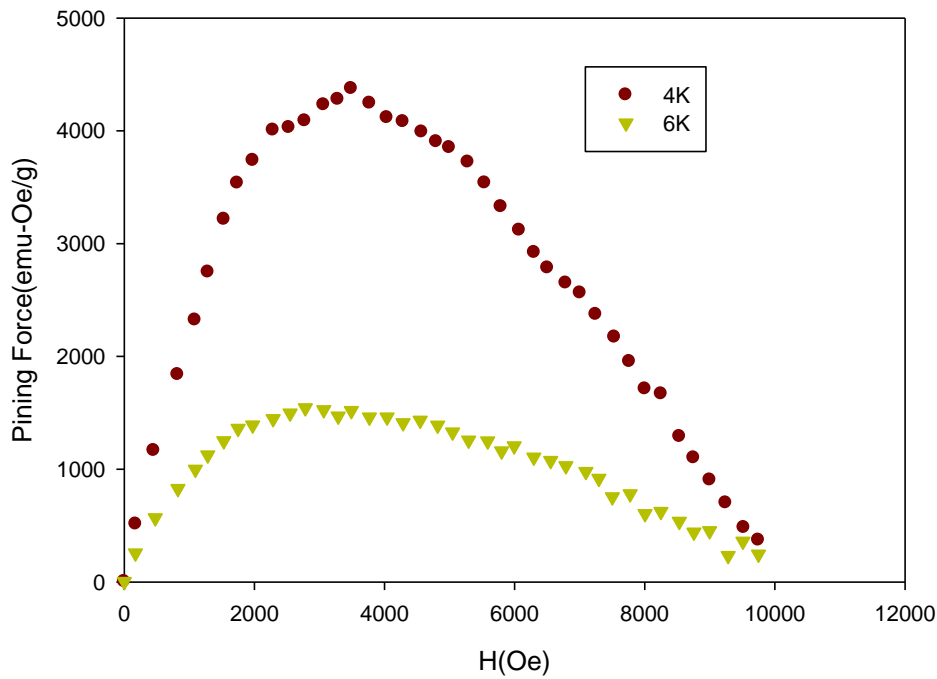


Figure 5.10: Variation of the pinning force with the applied field for set Q2_FeSeAs 6% of As

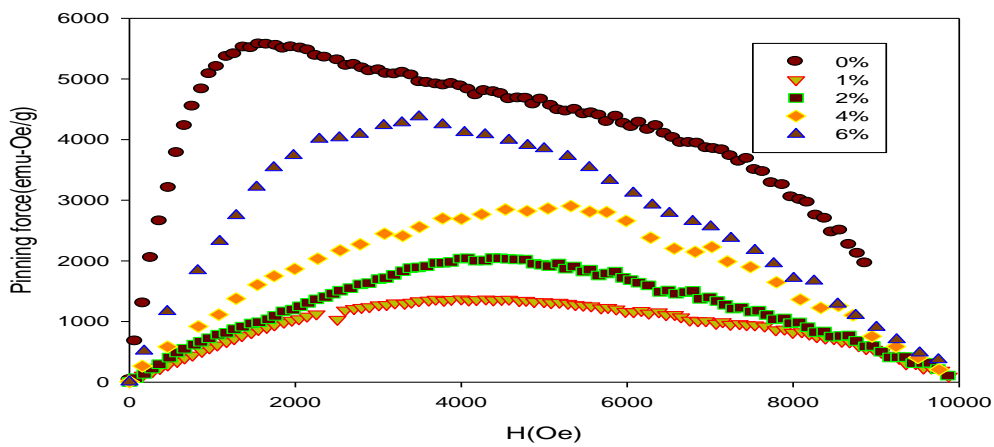


Figure 5.11: The trend of the variation of the pinning force for Set Q2-FeSeAs system at 4 K

The figures reveal that the trend of the pinning force with magnetic field is parabolic with reduction in the maximum pinning force as consequent upon increase in the concentration of arsenic. This parabolic behavior is similar what is reported in literature [36]. The figures show maximum at each temperature. When a flux line is shifted from a pinning center to unpinned position, work needs to be done. The work done in this case is referred to the pinning force per unit length of the pinning flux line [37]. The pinning force density is often obtained from the experimental data using $P_F = J_c X \mu_0 H$.

CHAPTER 6

CONCLUSION AND RECOMMENDATION

6.1 Conclusion

This thesis work investigates the effects of arsenic substitutions on the structural, transport, magnetic and superconducting properties of $\text{FeSe}_{1-x}\text{As}_x$ system. The samples were prepared using three different annealing and quenching procedures. X-ray diffraction patterns have been used to analyze various structural phases and calculate their lattice parameters. Little concentration of arsenic stabilizes tetragonal phases in set Q2 samples while hexagonal phases are promoted by arsenic in set Q3 samples. Points of inflection in resistivity-temperature graphs were differentiated to obtain the temperature at which the structural change occurs. Tetragonal phases further transformed to orthorhombic phases upon cooling the material down to temperature around 70 K. Likewise, the temperature at which the magnetic change occurs was obtained for each concentration of arsenic by differentiation points of inflection in magnetization-temperature graph.

The magnetic measurements reveal that the FeSeAs-system becomes ferromagnetic when the concentration of the arsenic gets to 8% while diamagnetic superconducting behavior was noted at the concentration below 8%. Critical current density as well as the pinning forces were estimated and found to decrease with the lowest concentration of arsenic. However, increase in the concentration of arsenic slightly raises the value of the critical current density but at a value lower than undoped material. The pinning forces for different concentrations of arsenic show a

decreasing pattern which makes one realize that the addition of arsenic lowers the pinning force and create room for the material to lose its superconductivity at a small value of current density.

Phase diagram of FeSeAs was established from the transport and magnetic measurement.

Further investigation on the lower concentrations of arsenic on FeSe system reveals the effect of iron particles in stabilizing the tetragonal phase that is responsible for superconductivity. In this case, addition of arsenic atoms to FeSe-system results into sudden destruction of superconductivity.

6.2 Recommendation for Future Work

1. One may consider investigating various properties of single crystals of FeSe doped with very small concentrations of arsenic. Anisotropic properties of the magnetization, critical current density and pinning forces may also be investigated.
2. Effects of elemental substitution on the Fe-sites is another possible way to investigate the corresponding magnetic, transport and structural effects.
3. Superconductivity in Cr-based materials.

Currently we already started investigating some of these projects in our lab.

References

- [1] Y. Kamihara, T. Watanabe, M. Hirano, and H. Hosono, “Iron-based layered superconductor $\text{La}[\text{O}(1-x)\text{F}(x)]\text{FeAs}$ ($x = 0.05\text{--}0.12$) with $T(c) = 26\text{ K}$.” *J. Am. Chem. Soc.*, vol. 130, no. 11, pp. 3296–7, Mar. 2008.
- [2] C. Bardeen, Leon, “Theory of Superconductivity*,” *PHYSICAL REV.*, vol. 108, pp. 1175–1204, 1957.
- [3] J. G. and K.A.Muller, “Possible High T_c superconductivity in the Ba-La-Cu-O System” *Phys.B-condensed Matter*, vol. 64, pp. 189–193, 1986.
- [4] M. Rotter, M. Tegel, and D. Johrendt, “Superconductivity at 38 K in the iron arsenide ($\text{Ba}_{1-x}\text{Fe}_x\text{As}$),” *Phys. Rev. Lett.*, vol. 2, pp. 2–5, 2008.
- [5] C. Day, “Iron based superconductors” *Phys. Today*, August, 2009.
- [6] Y. Mizuguchi, F. Tomioka, S. Tsuda, T. Yamaguchi, and Y. Takano, “Superconductivity at 27 K in tetragonal FeSe under high pressure” *Appl. Phys. Lett.*, vol. 93, no. 15, pp. 152505(1–3), 2008.
- [7] T.-K. Chen, J.-Y. Luo, C.-T. Ke, H.-H. Chang, T.-W. Huang, K.-W. Yeh, C.-C. Chang, P.-C. Hsu, C.-T. Wu, M.-J. Wang, and M.-K. Wu, “Low-temperature fabrication of superconducting FeSe thin films by pulsed laser deposition” *Thin Solid Films*, vol. 519, no. 5, pp. 1540–1545, Dec. 2010.
- [8] P. Min, F. Yong, C. Cuihua, and Z. Yong, “First-principles Study of Lattice, Magnetism and Electronic Structure for Fe-Based Superconductors: LaOFeAs , AFe_2As_2 ($\text{A}=\text{Sr}, \text{Ca}$), MFeAs ($\text{M}=\text{Li}, \text{Na}$) and FeSe ” *Rare Met. Mater. Eng.*, vol. 41, no. 8, pp. 1341–1345, Aug. 2012.
- [9] J. I. Gorina, G. a. Kaluzhnaya, M. V. Golubkov, V. V. Rodin, N. N. Sentjurina, and S. G. Chernook, “Growth and structure of superconducting FeSe crystals” *Crystallogr. Reports*, vol. 57, no. 4, pp. 585–589, Jul. 2012.
- [10] S. Margadonna, Y. Takabayashi, M. T. Mcdonald, K. Kasperkiewicz, Y. Mizuguchi, Y. Takano, and A. N. Fitch, “Crystal structure of the new FeSe $1-x$ superconductor \dagger ” *Chem. Commun.*, pp. 1–4.
- [11] C.-C. Chang, C.-H. Wang, M.-H. Wen, Y.-R. Wu, Y.-T. Hsieh, and M.-K. Wu, “Superconductivity in PbO-type tetragonal FeSe nanoparticles” *Solid State Commun.*, vol. 152, no. 8, pp. 649–652, Apr. 2012.
- [12] V. Romanovskii, “Temperature factor for magnetic instability conditions of type – II superconductors” *Phys. C Supercond.*, vol. 505, pp. 89–99, Oct. 2014.
- [13] J. Shimoyama, “Potentials of iron-based superconductors for practical future materials” *Supercond. Sci. Technol.*, vol. 27, no. 4, p. 044002, Apr. 2014.

- [14] X. C. Wang, Q. Q. Liu, Y. X. Lv, W. B. Gao, L. X. Yang, R. C. Yu, F. Y. Li, and C. Q. Jin, "The superconductivity at 18 K in LiFeAs system" *Solid State Commun.*, vol. 148, no. 11–12, pp. 538–540, Dec. 2008.
- [15] F.-C. Hsu, J.-Y. Luo, K.-W. Yeh, T.-K. Chen, T.-W. Huang, P. M. Wu, Y.-C. Lee, Y.-L. Huang, Y.-Y. Chu, D.-C. Yan, and M.-K. Wu, "Superconductivity in the PbO-type structure alpha-FeSe." *Proc. Natl. Acad. Sci. U. S. A.*, vol. 105, no. 38, pp. 14262–4, Sep. 2008.
- [16] S. Margadonna, Y. Takabayashi, Y. Ohishi, Y. Mizuguchi, Y. Takano, T. Kagayama, T. Nakagawa, M. Takata, and K. Prassides "Pressure evolution of the low-temperature crystal structure and bonding of the superconductor FeSe ($T_c=37$ K)," *Phys. Rev. B*, vol. 80, no. 6, p. 064506, Aug. 2009.
- [17] a. J. Williams, T. M. McQueen, and R. J. Cava, "The stoichiometry of FeSe" *Solid State Commun.*, vol. 149, no. 37–38, pp. 1507–1509, Oct. 2009.
- [18] a. Maeda, F. Nabeshima, H. Takahashi, T. Okada, Y. Imai, I. Tsukada, M. Hanawa, S. Komiya, and a. Ichinose "Synthesis, characterization, Hall effect and THz conductivity of epitaxial thin films of Fe chalcogenide superconductors," *Appl. Surf. Sci.*, vol. 312, pp. 43–49, Sep. 2014.
- [19] P. Kumar, A. Kumar, S. Saha, D. V. S. Muthu, J. Prakash, S. Patnaik, U. V. Waghmare, a. K. Ganguli, and a. K. Sood, "Anomalous Raman scattering from phonons and electrons of superconducting" *Solid State Commun.*, vol. 150, no. 13–14, pp. 557–560, Apr. 2010.
- [20] S. Demura, H. Okazaki, T. Ozaki, H. Hara, Y. Kawasaki, K. Deguchi, T. Watanabe, S. J. Denholme, Y. Mizuguchi, T. Yamaguchi, H. Takeya, and Y. Takano, "Electrodeposition as a new route to synthesize superconducting FeSe" *Solid State Commun.*, vol. 154, pp. 40–42, Jan. 2013.
- [21] B. H. Mok, C. L. Chen, H. H. Hsieh, S. M. Rao, T. W. Huang, C. L. Dong, M. C. Ling, W. C. Wang, M. K. Wu, and T. B. Wu, "Investigation of the structural distortion in FeSex crystals by X-ray absorption near edge structures (XANES) spectroscopy" *J. Phys. Chem. Solids*, vol. 72, no. 5, pp. 527–528, May 2011.
- [22] S. B. Zhang, H. C. Lei, X. D. Zhu, G. Li, B. S. Wang, L. J. Li, X. B. Zhu, W. H. Song, Z. R. Yang, and Y. P. Sun, "Divergency of SDW and structure transition in Fe $_{1-x}$ NixSe $_{0.82}$ superconductors" *Phys. C Supercond.*, vol. 469, no. 21, pp. 1958–1961, Nov. 2009.
- [23] W. Wang, J. Sun, S. Li, and H. Lu, "Electronic structure and phonon spectrum of binary iron-based superconductor FeSe in both nonmagnetic and striped antiferromagnetic phases," *Phys. C Supercond.* vol. 472, no. 1, pp. 29–33, Jan. 2012.
- [24] Y. Mizuguchi, F. Tomioka, S. Tsuda, T. Yamaguchi, and Y. Takano, "FeTe as a candidate material for new iron-based superconductor," *Phys. C Supercond.* vol. 469, no. 15–20, pp. 1027–1029, Oct. 2009.
- [25] G. Rahman, I. Gee Kim, and A. J. Freeman, "First-principles prediction of spin-density-reflection symmetry driven magnetic transition of CsCl-type FeSe" *J. Magn. Magn. Mater.*, vol. 322, no. 20, pp. 3153–3158, Oct. 2010.

- [26] M. Pan, H. F. Ma, J. T. Zhu, C. H. Cheng, Z. Huang, Y. Zhang, H. Zhang, and Y. Zhao, “Distorted magnetic orders and electronic structures for FeSe under pressure” *Phys. C Supercond.*, vol. 471, no. 21–22, pp. 603–607, Nov. 2011.
- [27] M. W. Ma, D. N. Yuan, Y. Wu, X. L. Dong, and F. Zhou, “Crystal growth of iron-based superconductor FeSe_{0.94} by KCl flux method” *Phys. C Supercond. its Appl.*, vol. 506, pp. 154–157, Nov. 2014.
- [28] X. Li, Z. Gao, Y. Liu, Z. Ma, L. Yu, H. Li, and H. Yang, “The microstructures and superconducting properties of FeSe_{0.5}Te_{0.5} bulks with original milled powders” *Cryogenics (Guildf)*., vol. 57, pp. 50–54, Oct. 2013.
- [29] T. B. Massalki, “Binary alloy of phase diagram.” Second edition. vol. 1 and 2 .
- [30] M. M. Shivastava and O. N. Srivastava, “Studies of structural transformations and electrical behaviour of FeSe films” *Thin Solid Films*, vol. 29, no. 2, pp. 275–284, Oct. 1975.
- [31] S. K. Yadav, Anil K, “Effect of nominal substitution of transition metals for excess Fe in Fe_{1+x}Se superconductor” *arXiv:1405.2050v1 [cond-mat.supr-con]*, pp. 1–16, 2014.
- [32] D. Mendoza, J. L. Benítez, F. Morales, and R. Escudero, “Magnetic anomaly in superconducting FeSe” *Solid State Commun.*, vol. 150, no. 25–26, pp. 1124–1127, Jul. 2010.
- [33] D. Dew-Hughes, “The critical current of superconductors: an historical review” *Low Temp. Phys.*, vol. 27, no. 9, p. 713, Sep. 2001.
- [34] C. S. Yadav and P. L. Paulose, “The flux pinning force and vortex phase diagram of single crystal” *Solid State Commun.*, vol. 151, no. 3, pp. 216–218, Feb. 2011.
- [35] D. Laan and V. Eck, “Temperature and magnetic field dependence of the critical current of Bi₂Sr₂Ca₂Cu₃O_Xtape conductors” *Trans. Appl. Supercond.*, vol. 1, no. I, pp. 3345–3348, 2001.
- [36] C. S. Yadav, P. L. Paulose, and M. Sciences, “The flux pinning force and vortex phase diagram of single crystal” *Solid state communications*.vol. 2, pp.216-218,2011
- [37] F. Ben Azzouz, M. Zouaoui, a. Mellekh, M. Annabi, G. Van Tendeloo, and M. Ben Salem, “Flux pinning by Al-based nanoparticles embedded in YBCO: A transmission electron microscopic study” *Phys. C Supercond.*, vol. 455, no. 1–2, pp. 19–24, May 2007.

VITAE

Name : Owolabi Taoreed Olakunle

Nationality : Nigerian

Date of Birth : 15th Dec, 1985

Email : owolabitaoreedolakunle@gmail.com

Telephone : +966556202152;+2348067226208

Address : Physics and Electronics Department, Adekunle
Ajasin Akungba Akoko. Nigeria

Conference Presentation : Khalil .A. Ziq, Taoreed.O. Owolabi and A.F Salem, “On the phase diagram of FeSe doped superconductor” April 29, 2014. 4th international conference on superconductivity and magnetisms, Turkey.

Khalil .A. Ziq, Taoreed. O. Owolabi, A.F Salem and K. Shankar, “On the magnetic and superconducting state of FeSe superconductor” July, 2014. International conference on spin-polarized scanning tunneling microscopy Sawmill Creek Resort, Huron. Ohio. United State.

Khalil .A. Ziq, Taoreed. O. Owolabi: On the phase Diagram of FeSe_{1-x}As_x . APS march meeting, March 2-6, 2015. SAN ANTONIO

